

SECRET

TL: 14-58/DS

CONFIDENTIAL

A BRIEF TECHNICAL DESCRIPTION OF THE AVROCAR

AVRO/SPG/TR174



AVRO AIRCRAFT LIMITED

CONFIDENTIAL

SECRET

I.D. 58RDZ-16141

SECURITY WARNING

This document is intended solely for the recipient and such persons as have been delegated to use it in the course of their duty, and may be used in connection with work performed for or on behalf of the United States Air Force.

The transmission, unauthorized retention, destruction, or the revelation of its contents, in any manner, to any unauthorized persons(s) is forbidden.

Failure to comply with any of the above instructions is an infraction of the Canadian Official Secrets Act and is a violation within the meaning of the United States Espionage Laws, title 18, U.S.C. sections 793 and 794.

To:

K.L.

Date:

Copy No: **33**

I.D. No. 58RDZ-16141

*Re-classified as per
SRCA dated 15th Oct
1959*

*P.28 Missing
from original*

SECRET

SPECIAL PROJECTS GROUP
Technical Report No. 174

A BRIEF TECHNICAL DESCRIPTION OF THE AVROCAR

May 1958

Issued by:

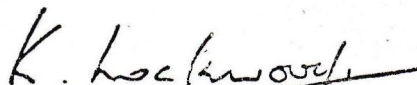
Avro Aircraft Limited
Malton, Ontario, Canada

under

Supplementary Agreement No. 3
to Contract No. AF33(600)30161


Prepared by:


D. C. Whitteley
Avro Aircraft Limited


K. Lockwood
Avro Aircraft Limited

Approved by:


J. C. M. Frost
Chief Design Engineer
Special Projects Group
Avro Aircraft Limited


T. D. Earl
Chief Aerodynamicist
Special Projects Group
Avro Aircraft Limited

The number of pages included in this report, including Security Warning, Title Page, Table of Contents, is 45.

SECRET

I.D. No. 58RDZ-16141

TABLE OF CONTENTS

<u>Section</u>	<u>Title</u>	<u>Page No.</u>
1.0	SUMMARY	1
2.0	INTRODUCTION	1
3.0	DESCRIPTION OF AIRCRAFT	1
4.0	WEIGHT SUMMARY	2
5.0	PERFORMANCE ESTIMATES	4
6.0	STABILITY AND CONTROL CHARACTERISTICS	12
7.0	LIST OF SYMBOLS	14
8.0	REFERENCES	16
9.0	TABLES I, II AND III	17
10.0	LIST OF ILLUSTRATIONS	19

1.0 SUMMARY

This report provides a brief outline of the technical aspects and performance of the Avrocar (Ref. 1). It contains a short description of the aircraft to brief those unfamiliar with the project.

An attempt is made to substantiate the technical claims as far as possible within the limits of present knowledge. More detailed reports on each aspect of the work will be forthcoming as studies and tests on the project proceed.

2.0 INTRODUCTION

The Avrocar is a new type of VTOL aircraft suitable for operating at low speeds close to the ground and also capable of speeds in excess of 250 knots at altitudes up to 10,000 ft. The design is derived from a supersonic aircraft with VTOL capability projected by Avro Aircraft Limited and much of the research work already carried out for the supersonic aircraft is directly applicable to the subsonic Avrocar.

3.0 DESCRIPTION OF AIRCRAFT

Fig. 1 is a three-view general arrangement of the vehicle. It is an all wing design of circular planform approximately 18 ft. in diameter. In section the wing is a cambered ellipse with thickness to chord ratio of approximately 20 percent.

The wing section is symmetrical about the vertical centerline, resulting in a very simple radial structure. The vehicle stands approximately 5 in. off the ground, has an overall height of 4.8 ft. and will take-off vertically at a weight of 5,650 lb. which includes a payload of 2,000 lb. and fuel for over 100 miles flight.

Three Continental J69-T9 turbojets (927 lb. S.L. static thrust, 27 in. overall diameter, 364 lb. weight) are symmetrically disposed in plan with their exhausts directed inboard (Ref. Fig. 2). The exhaust is collected in a tusk-like chamber and directed through nozzle guide vanes to impinge upon turbine blades attached at the outer edge of the turborotor assembly. (Fig. 3)

The turborotor (Ref. Fig. 4) draws in air through a circular intake from the wing upper surface and forces it radially outwards through diffuser ducts in the main structure (Ref. Fig. 1). Some of the air forced out by the turborotor is directed back to feed the turbojets, but the

3.0 DESCRIPTION OF AIRCRAFT (continued)

main flow is expelled from an annular nozzle at the wing periphery. A proportion of this main flow escapes from an inner annulus. This is done to stabilize the ground cushion.

The peripheral jets are directed downwards for take-off and this annular jet in the presence of ground provides an appreciable thrust augmentation. This is known as the ground cushion effect and the approximate flow pattern close to the ground is illustrated in Fig. 5.

The vehicle may be operated to hover or move within the ground cushion. Transition to forward flight is effected by gradually deflecting some of the jet flow from the peripheral nozzles to the rear. The vehicle accelerates forward, and is inclined upward. The jet sheet at the rear of the wing induces a very large lift coefficient which, together with the low wing loading, enables the wing to support the entire weight of the vehicle at a speed of 45 mph. In landing, descent is made at constant power until the presence of the ground is sensed as the vehicle enters the ground cushion. The throttle is then progressively closed to settle the vehicle onto the ground.

The aircraft control system is described in Section 6.0 below.

4.0 WEIGHT SUMMARY

Details of the estimated component weights are given for the following groups:

- (i) Structure
- (ii) Landing gear
- (iii) Powerplant
- (iv) Fixed services
- (v) Useful load

Total weights may be summarized as follows:

Weight empty	2820 lb.
Useful load	2830 lb.
GROSS WEIGHT	5650 lb.

4.0 WEIGHT SUMMARY (continued)

where useful load is made up as follows:

Crew members	400 lb.
Fuel	780 lb.
Oil	37 lb.
Payload	1613 lb.
TOTAL USEFUL LOAD	<u>2830 lb.</u>

4.2.1 Group #1 Structure

	<u>Weight lb.</u>
Wing	535
Air Intake	26
Propulsion Ducting	52
Access Panels	50
Cockpit Canopy	35
Engine Bay Cowlings	24
TOTAL STRUCTURE	<u>722</u>

4.2.2 Group #2 Landing Gear

TOTAL LANDING GEAR	70 lb.
--------------------	--------

4.2.3 Group #3 Powerplant

Impeller	117
Impeller Shaft & Turbine Casing	181
Impeller Oil System	4
Engine Marbores J69-T-9	1092
Fire Walls	10
Engine Installations	12
Engine Oil System	18
Intake Diffusers	—
Exhaust Diffusers	108
Engine Fuel System	77
TOTAL POWERPLANT	<u>1619 lb.</u>

4.2.4 Group #4 Fixed Services

Flying Controls	116
Pneumatics	48
Vacuum System	—
Cockpit Furnishings	49
Engine Controls	13
Radio and Intercom.	25
Engine Instruments	12
Propulsion Instruments	1
Flight Instruments	9
Navigation Instruments	2

4.0 WEIGHT SUMMARY

4.2.4 Group #4 Fixed Services (continued)

Weight lb.

Electric Power Supply	72
Flying Controls Electrics	8
Engine Starting Electrics	41
Engine Instruments Electrics	10
Propulsion Instruments Electrics	1
Cargo Bay Floors	—
Cargo Bay Mooring Equipment	—
A/C Jacking Pads & Mooring Equipment	—
Air Conditioning	2
TOTAL FIXED SERVICES	<u>409</u>

4.2.5 Group #5 Useful Load

Crew Members	400
Residual Fuel	13
Fuel	767
Trapped Oil	2
Oil	35
Payload	1613
TOTAL USEFUL LOAD	<u>2830</u>

5.0 PERFORMANCE ESTIMATES

Wherever possible the basis of prediction has been explained but estimates must be considered as preliminary only.

The subject is described under the following headings:

1. Engine Performance
2. Aircraft Drag Estimate
3. Aircraft Performance

5.1 Engine Performance

Although the coupling between gas generator and fan for equilibrium running is slight the 'closed loop' nature of the engine cycle nevertheless, makes the component matching a lengthy task. Certain simplifying assumptions have therefore been made in order to save time.

The design point calculation is given in Table I. This corresponds to maximum power at sea level and zero forward speed.

5.0 PERFORMANCE ESTIMATES

5.1 Engine Performance (continued)

For the purpose of preliminary estimation it has been assumed that the pressure ratio across the fan (P_3/P_2) remains constant with forward speed. The gas generators are, in effect, supercharged by the fan and by ram pressure. Intake pressure recovery (P_2/P_1) falls away from 1.0 at zero forward speed to 0.97 at $M = 0.4$ (see Fig. 6). Effect of altitude has been accounted for by allowing the thrust and fuel flow to vary linearly with density - this is in accordance with previous experience on this type of powerplant.

For in-flight cases the gross thrust has been reduced by 10 percent. to allow for nozzle or cosine losses, and for jet drag (see 5.2.6).

A sample calculation of thrust variation with forward speed is given in Table II.

The basis of powerplant performance at reduced power settings is given in Table III. Variations of net thrust and fuel flow with forward speed at sea level, 10,000 ft. and 20,000 ft. have then been evaluated for the following cases:

- (i) 3 Continental J-69-T9 engines at 22,700 rpm (max. power).
- (ii) 3 Continental J-69-T9 engines at 21,000 rpm (normal power).
- (iii) 3 Continental J-69-T9 engines at 19,150 rpm (75% normal power)

Variations of net thrust in terms of (F_n/p_a) for all conditions are given in Fig. 13. Corresponding values of fuel flow (W_f/p_a) are found in Fig. 7.

5.2 Aircraft Drag Estimate

The drag of the aircraft can be broken down into the following components.

- 1. Wing Drag
- 2. Canopy Drag
- 3. Landing Gear Drag
- 4. Interference Drag
- 5. Drag due to Surface Imperfections
- 6. Jet Drag
- 7. Lift Induced Drag

5.0 PERFORMANCE ESTIMATES (continued)

5.2.1 Wing Drag

From the Royal Aeronautical Society data sheets it is possible to determine the profile drag of smooth wings using the relation

$$C_{D_0} (\text{wing}) = \lambda C_{D_0} (\text{flatplate})$$

where λ = ratio of profile drag coefficient of the wing to that of the corresponding flat plate at the same Reynolds number and transition point.

$$\text{The wing Re. No.} = \frac{V \bar{c}}{\nu}$$

$$\text{Where } \bar{c} = S/b = 254.5/18 = 14.14 \text{ ft.}$$

for a typical cruising speed of 200 knots at S.L.
Re. No. = 3.03×10^7

and to make a fairly conservative estimate it will be assumed that the transition point occurs at the wing leading edge.

Hence from R.Ae.S. data sheet wings 02.04.01.

$$C_{D_0} (\text{flatplate}) = 0.005$$

From R.Ae.S. data sheet wings 02.04.02 for a wing with maximum thickness at 0.5c, $t/c = 0.20$ and convex trailing edges

$$\lambda = 1.72$$

$$\therefore C_{D_0} (\text{wing}) = 1.72 \times 0.005 \\ = 0.0086$$

It is necessary to make some allowance for the fact that the wing has an elliptic section trailing edge instead of sharp convex. The increase in drag due to the blunt trailing edge will, however, be partially reduced by the jet efflux. As a first approximation it will be assumed that the preceding wing drag coefficient is increased by 20 percent. so that

$$C_{D_0} (\text{wing}) = 0.0103$$

5.2.2 Canopy Drag

Ref. 2 gives the drag of conventional type canopies for subsonic aircraft as being between $CD = 0.05$ and $CD = 0.15$ based on frontal area (see Fig. 4, Chpt. 13-2 of this Ref.). However Ref. 2 also shows that

5.0 PERFORMANCE ESTIMATES

5.2.2 Canopy Drag (continued)

the drag of a canopy increases sharply for length to height ratios of less than 8. Since the Avrocar canopies have length to height ratios of approximately 2.8 it would seem reasonable to take the highest value of the drag coefficient range quoted above i.e. $C_D = 0.15$.

The frontal area of each canopy is 2.08 sq. ft.

Hence the drag coefficient based on wing area for both canopies is $C_{D0} = 0.0024$.

5.2.3 Landing Gear Drag

The landing gear for drag estimation purposes can be considered equivalent to two high fineness ratio fairings. From Ref. 2 it is shown that the drag coefficient of fairings with high fineness ratios (greater than 10) can be approximated by

$$C_D = 0.002 \ell/h \text{ based on frontal area.}$$

$$\ell/h = 21$$

$$\text{hence } C_D = 0.042 \text{ based on frontal area.}$$

Total frontal area of landing gear = 0.53 sq. ft.

$$\text{Hence } C_D = 0.042 \times 0.53/254.4 = 0.0001$$

5.2.4 Interference Drag and Drag due to Surface Imperfections

5.2.5

These components drags are difficult to estimate accurately. Interference drag should be small since there are no wing or tail to fuselage junctures. An allowance of 8% of the total will be made for these items.

5.2.6 Jet Drag

The data of Ref. 3 show that a jet drag was measured. Due to some inconsistency the exact value is difficult to determine but it appears to be between 2% and 6% of the gross thrust. Since it is proportional to gross thrust it is more easily taken care of as a thrust reduction and is included in the allowance under 5.1.

Zero lift drag coefficient is then

$$C_{D0} = 0.0103 + 0.0024 + 0.0001 + 0.08 C_{D0} = .014$$

5.0 PERFORMANCE ESTIMATES (continued)

5.2.7 Induced Drag

In estimating the lift induced drag it was possible to make use of the aerodynamic data given in Ref. 3. This reference gives the results and analysis of the subsonic tests which were made on a circular plan form model with peripheral jets. Fig. 8 shows a plot of C_D versus C_{Ltrim} for various values of jet coefficient, C_j , which has been derived from these results. Replotting the results as C_D versus C_L^2 in Fig. 9 shows that the points lie almost on a straight line for $0.25 \leq C_j \leq 0.35$. It is therefore possible to represent the drag in a conventional manner for this C_j range.

$$\text{i.e. } C_D = C_{D0} + C_L^2 / (\pi A e)$$

From Fig. 9 $dC_D/dC_L^2 = 1/(\pi A e) = 0.312$ giving $e = 0.80$

hence $C_D = C_{D0} + 0.312 C_L^2$ for $0.25 \leq C_j \leq 0.35$

(A typical value of C_j for the Avrocar at $M = 0.3$, S.L. and maximum power is 0.32). It seems reasonable, in the absence of any other data, to assume that dC_D/dC_L^2 will be approximately the same for the Avrocar.

It is important to realize that the drag coefficient is here defined by:

$$C_D = C_j - C_{F-D} - mV/qS$$

using the notation of Ref. 3.

This means that variation of jet drag with angle of attack and thrust loss due to trimming have been accounted for by an adjustment to the value of drag efficiency factor.

Total Drag

Hence drag of the Avrocar to a first approximation and in the absence of test results is given by

$$C_D = 0.014 + 0.312 C_L^2$$

5.3 Aircraft Performance

For convenience the performance estimates will be dealt with under the following headings:

1. Hovering Performance
2. Level Flight Performance
3. Climb Performance
4. Range for Various Take-off Conditions

5.0 PERFORMANCE ESTIMATES (continued)

5.3.1 Hovering Performance

It is necessary to consider the aircraft hovering in two conditions:

- (a) When the effect of the 'ground cushion' is present i.e. from zero to approximately 0.9 spans above the ground.
- (b) Hovering in free air.

In case (a) the annular jet from the wing is bent outwards due to the presence of the ground. Ref. 4 shows how this results in a pressure on the wing undersurface which is greater than ambient pressure. This pressure differential causes an upward force on the wing in addition to that of the jet reaction. Hence we can define a thrust augmentation factor where:

$$n = \frac{\text{total vertical thrust}}{\text{theoretical free air nozzle thrust}}$$

A plot of n versus height above the ground in spans is shown in Fig. 10. This plot has been derived from the results of model measurements given in Ref. 5.

In case (b) when the ground effect is not present, the annular jet tends to collapse into a 'solid' jet resulting in pressures on the wing undersurface which are lower than ambient so that n becomes less than one. This adverse effect may be minimized by providing a few small gaps in the "jet curtain" and under such conditions the value of n becomes about 0.9.

For hovering in either case (a) or (b)

$$n F_0 = W$$

where F_0 = static thrust and W = aircraft weight

Since part of the thrust must be used for control or transition to forward flight, it will be assumed that only 96 percent. is available for hovering so that

$$0.96 n F_0 = W$$

The payload which the aircraft can carry in the hovering condition is then calculated simply:

$$\text{Payload} = 0.96 n F_0 - (\text{aircraft empty weight} + \text{oil weight} + \text{fuel weight})$$

(payload as defined in this equation includes the weight of crew).

5.0 PERFORMANCE ESTIMATES

5.3.1 Hovering Performance (continued)

In order to calculate the hovering performance when the aircraft takes off from an airstrip at 6,000 ft. pressure altitude and with an ambient temperature of 90° it has been assumed that

$$F'_0 = \text{constant} \times t_a/p_a$$

$$\text{Hence } F'_0 = F_0 \times p_a'/p_a \cdot t_a/t_a'$$

where the symbols with the dash indicate non-standard conditions and symbols without dash indicate S.L. standard conditions.

Hence at 6,000 ft. and 90°F, $F'_0 = 0.756 F_0$

A plot of payload versus hovering height above the ground is shown in Fig. 11.

The hovering endurance with 1,000 lb. payload was calculated as follows:

$$\text{thrust required} = F_0 = \frac{\bar{W}}{0.96n}$$

where \bar{W} = mean aircraft weight

if W_f is the fuel flow corresponding to F_0

then the endurance = weight of fuel carried/ W_f

The hovering endurance is shown in Fig. 12.

5.3.2 Level Flight Performance

The level flight performance was determined from plots of F_N/p_a and D/p_a versus Mach number where F_N/p_a is given in Table II and D/p_a can be derived from the drag equation given in Section 5.2 as follows:

$$C_D = 0.014 + 0.312 C_L^2$$

$$D/p_a = \gamma/2 M^2 S C_D$$

$$D/p_a = \gamma/2 M^2 S (0.0140 + 0.312 C_L^2)$$

but in level flight

$$C_L = W/(\gamma/2 p_a M^2 S)$$

$$\text{thus } D/p_a = 0.0140 \gamma/2 M^2 S + 0.312 (W/p_a)^2 / (\gamma/2 M^2 S)$$

for $\gamma = 1.4$ and $S = 254.5$ sq. ft.

$$D/p_a = 2.49 M^2 + (0.00175/M^2)(W/p_a)^2$$

5.0 PERFORMANCE ESTIMATES

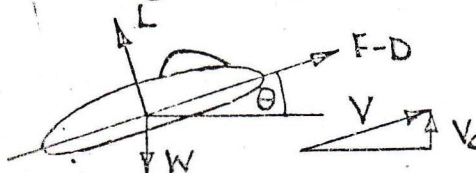
5.3.2 Level Flight Performance (continued)

Plots of D/p_A versus M for various values of W/p_A have been superimposed on the thrust curves shown in Fig. 13. (This non-dimensional method of presentation has been chosen since only one set of drag curves are required to include the effects of aircraft weight and altitude). From Fig. 13 and using the fuel flow data given in Section 5.1, the following plots have been derived to illustrate the level flight performance at three representative aircraft weights:

- (a) Maximum speed versus altitude - Fig. 14.
- (b) Specific air range versus true air speed for various engine rpm at S.L. and 10,000 ft. - Fig. 15 and 16.

5.3.3 Climb Performance

Referring to the diagram below:



resolving along the flight path $W/g(dV/dt) = F-D - W \sin \theta$

If dV/dt is neglected then $\sin \theta = (F-D)/W$

The rate of climb $V_c = V \sin \theta \therefore V_c = [(F-D)/W] V$

As a first approximation it can be assumed that $L \approx W$ and Fig. 13 can be used to find $(F-D)/W$ since

$$(F-D)/W = [(F-D)/p_A] \times 1/(W/p_A)$$

If maximum engine rpm is used for the climb, the best rate of climb is achieved at a speed of $M = 0.27$.

Fig. 17 and 18 show the estimated rate of climb versus altitude and the time to height respectively.

5.3.4 Range for Various Take-off Conditions

Fig. 19 illustrates the range versus true airspeed for three typical loading conditions. Fig. 20 shows a plot Payload versus Range.

6.0 STABILITY AND CONTROL CHARACTERISTICS

6.1 Introduction

The aircraft is of circular planform and the fan delivers air equally to each sector. Exhaust nozzles at the periphery are designed to deflect the jet to provide both control and damping of the aircraft. Damping signals are provided by the rotor which acts as a gyroscope and control deflections for trim are provided by the pilot. It may be necessary to stabilize the long period motion by means of signals from a device known as the 'q' box, which senses changes in speed. This will not, however, be fitted to the first aircraft.

6.2 Description of Control System

Since the aircraft is basically unstable, a full-time automatic control system is incorporated. The principle of operation of this system is derived from the fact that an unstable aircraft can be stabilized in pitch and roll (except for a slow divergence) if the aircraft incorporates a rotor of sufficient angular momentum mounted with the axis vertical. Since the fan in the System 606A aircraft is not large enough for this purpose, it is used to activate the control system such that the control moment amplifies the gyrocouple produced by the fan. This is done by mounting the rotor shaft on a spherical bearing and connecting the free end to a spring loaded linkage which operates the jet controls in the appropriate manner. In fact, the turbo-rotor is allowed to pitch and roll a very small amount within the vehicle. The relative motion is stepped up with flexural linkage into a control post and this is connected directly to the jet controls through a number of cables. The operator's controls also act on the post through pneumatic bellows. Thus when the aircraft is pitching or rolling, a correction is applied by the controls but the pilot always obtains manoeuvre by overriding the stabilizer. The change in jet direction as the vehicle pitches, performs the same function as the fixed stabilizer of a conventional aircraft.

Fig. 21 shows a schematic of the gyro damping system and Fig. 22 illustrates the control nozzle mechanism. The jets are deflected at the periphery by means of small spoilers fitted in the throat of the annular nozzle. The nozzles cause the jet to bend by the Coanda effect either up or down. If the upper and lower spoilers project equally at the throat the jet exhausts radially. By suitable means the jet at the front and at the wing tip are made to provide forward thrust for the in-flight case. Similarly during transition, the weight is supported as required by a combination of jet and aerodynamic lift.

6.0 STABILITY AND CONTROL CHARACTERISTICS

6.2 Description of Control System (continued)

The operator controls pitch and roll by means of a conventional control stick. The total movement of the spoilers is small (0.25"). They are flexure mounted and very light in weight and the jet responds almost immediately to the spoiler position so that a very rapid response is possible. This feature is essential to the satisfactory performance of the stabilizer. Equally essential, is the fact that the stabilizer must not compromise safe operation of the controls and therefore this simple direct system which depends upon the turborotor acting as a gyro is used.

To take-off, the peripheral jets are directed downwards by means of a screw jack which lowers the spoilers collectively and produces the vertical curtain of air referred to above, (see Fig. 5). From the diagram it will be seen that this action does not affect the stabilizer or the pilot's normal pitch and roll control.

6.3 In-flight Characteristics

The equations of motion of the aircraft in forward flight have been written for small perturbations from an initially straight flight path. These equations have been set up on an analog computer and preliminary results have been obtained for level flight at sea level, at Mach numbers of 0.15 and 0.40. Static longitudinal aerodynamic characteristics were derived from the results of tests on the 1/6 scale reflection plane model (see Ref. 3). Lateral and dynamic derivatives were estimated since no data were available.

It should be noted that the momentum drag coefficients assumed in the derivation of these characteristics were substantially less than those which will be obtained with the Avrocar. The significance of this is that a larger momentum drag coefficient will result in a larger thrust coefficient, which will increase the control power. Also, the physical shape of the Avrocar differs somewhat from that of the 1/6 scale model in that the Avrocar has more camber, a thicker section and a rounded edge instead of a sharp edge. The effect of these differences can not be accurately predicted at the present time.

Subject to these provisions, the analog records shown in Figs. 23 and 24 indicate the response of the Avrocar to a sharp-edged vertical up-gust. The initial flight conditions were level unaccelerated flight at sea level, at flight Mach numbers of 0.15 (Fig. 21) and 0.40 (Fig. 22). These traces represent the response for gusts of

6.0 STABILITY AND CONTROL CHARACTERISTICS

6.3 In-flight Characteristics (continued)

any velocity less than the minimum velocity required to cause the control to reach the limit, and the scales have been arranged to show the ratio of each variable to the gust velocity. This representation is possible because within the control limits the equations are linear. The gust velocity required to produce a divergence due to lack of sufficient control power exceeds the above "linearity limit" by a considerable margin, and both limits will be increased by increasing the thrust coefficient (see above) and/or introducing gusts with finite gradient lengths.

The response may be conveniently considered in two parts, namely, an initial fairly rapid motion including some oscillation, particularly in the control variables, and a long-period oscillation similar to the "phugoid" mode of a conventional aircraft. In order to adequately display both modes two records are shown for each case. The cross-coupling effect of the control system is evident in the response of roll angle ϕ and roll control J_a to the vertical gust. The initial overshoot on angle of attack due to the negative static margin will be noted. The stabilization of the long period mode by the Q-jack is clearly shown.

These data provide an idea of the response characteristics obtained from the first preliminary analysis. It is important to note that the results do not include effect of pilot correction. The next phase of the simulation study will include pilot input.

7.0 LIST OF SYMBOLS

b	Span	(ft.)
c	Root chord	(ft.)
\bar{c}	S/b	(ft.)
D	Drag force	(lb.)
e	Oswald efficiency factor	
F	Propulsive force	(lb.)
F_s	Longitudinal force	(lb.)
J_a	Roll control parameter	
J_e	Pitch control parameter	

7.0 LIST OF SYMBOLS (continued)

L	Lift force	(lb.)
M	Mach number	
m	Mass flow	(slugs/sec.)
n	Thrust augmentation factor	
P	Total pressure	(lb./sq.ft.)
p	Static pressure	(lb./sq.ft.)
Q	Mass flow	(lb./sec.)
Re	Reynolds number = $V\bar{c}/\nu$	
S	Plan form area	(sq.ft.)
Δu	Forward speed perturbation	(ft./sec.)
V	Velocity	(ft./sec.)
V_c	Rate of climb	(ft./sec.)
V_G	Gust velocity	(ft./sec.)
W	Weight	(lb.)
W_f	Fuel flow	(lb./hr.)
α	Angle of attack	(deg.)
γ	Ratio of specific heats	
θ	Angle of climb (perturbation for analog results)	
ϕ	Roll angle	
ρ	Density	(slugs/cu.ft.)

Aerodynamic Coefficients

C_D	Drag coefficient D/qS
C_{D_0}	Profile drag coefficient
C_{D_e}	Induced drag coefficient
C_{F-D}	Net propulsive force coefficient $F-D/qS$

7.0 LIST OF SYMBOLS (continued)

Aerodynamic Coefficients

- C_L Lift coefficient L/qS
 C_j Jet coefficient $F_j (J_{e=0})/qS$
 mV/qS Momentum drag coefficient

Other Suffices

- a Ambient
n Net
1 Engine inlet
2 Fan inlet
3 Fan outlet
6 Peripheral nozzle outlet

8.0 REFERENCES

1. Model Specification - Avrocar I
2. Fluid-dynamic Drag - S. F. Hoerner (1958)
3. Presentation and Discussion of Sixth-scale Model Subsonic Test Results - Project 1794
AVRO/SPG/TR12
4. Theory of the Annular Nozzle in Proximity to the Ground - David W. Taylor, Model Basin Aero. Laboratory Report 923
5. Air Cushion Effect Tests Part 2 - AVRO/SPG/TR29
6. The Royal Aeronautical Society data sheets - Aerodynamics Vol. 2.

9.0

TABLE I

AVROCAR POWERPLANT - GAS DYNAMIC DESIGN BASIS

Engines	Continental J-69-T9
Design air mass flow (total air)	550 lb./sec.
(Note - Engines breathe from end of radial diffuser duct)	
Loss to main compressor face	negligible
For first bend	$\Delta P/q_{inlet} = 0.10$
For radial diffuser duct	$\Delta P/q_{inlet} = 0.144$
For engine inlet to compressor eye	$\Delta P/q_{inlet} = 0.213$
For engine outlet diffuser duct	
loss up to nozzle guide vane	
(additional to normal jet pipe loss)	$\Delta P/P = 0.05$
For power turbine outlet duct loss	$\Delta P/P = 0.01$
Compressor temperature rise	$T_3 - T_2 = 9.0 \text{ deg C}$
Compressor work done = turbine	
work done	$= 1188 \text{ Chu/sec.}$
Compressor efficiency	$\eta_c = 0.88$
Compressor pressure ratio	$P_3/P_2 = 1.09965$
First bend pressure recovery	$P_4/P_3 = 0.9898$
Central nozzle pressure ratio	$P_a/P_4 = 0.91877$
Central nozzle area	$A_{e4} = 576 \text{ in.}^2$
Central nozzle airflow	$Q_C = 119.2 \text{ lb./sec.}$
Central nozzle thrust	$X_{GC} = 1452 \text{ lb.}$
Radial duct pressure recovery	$P_5/P_4 = 0.99$
Engine inlet pressure recovery	$P_6'/P_5 = 0.99$
Engine overall pressure ratio	$P_7'/P_6' = 1.646$
Engine outlet temperature	$T_7' = 954 \text{ deg K}$
Engine outlet duct recovery	$P_8'/P_7' = 0.95$
Power turbine pressure ratio	$P_8'/P_9' = 1.5337$
Power turbine efficiency	$\eta_t = 0.825$
Power turbine temperature drop	$H_S = 78.66 \text{ deg C}$
Power turbine gas flow	$Q_E = 54.72 \text{ lb/sec}$
Peripheral nozzle gas flow	$Q_P = 430 \text{ lb./sec.}$
Peripheral nozzle pressure recovery	$P_6/P_5 = 0.9865$
Peripheral nozzle pressure ratio	$p_a/P_6 = 0.94075$
★ Peripheral nozzle outlet temperature	$T_6 = 380 \text{ deg K}$
Peripheral nozzle thrust	$X_{GP} = 5048$
Peripheral nozzle area	$A_{e6} = 2784 \text{ in.}^2$
Total thrust	$X_{TOT} = 6500 \text{ lb.}$
Total nozzle area	$A_e = 3360 \text{ in.}^2$

★ NOTE

- (1) The primary and secondary flows mix in the diffuser duct, however the gas generator inlet duct breathes unvitiated air since deflector ducting carries the turbine exhaust to the adjacent peripheral exhaust ducts.

SECRET

AVRO/SPG/TR174

18.

9.0 (continued)

- (2) A proportion (12.5 percent) of the total airflow is exhausted from a central annular nozzle arrangement in order to stabilize the aircraft while hovering in the ground cushion. This reduces the radial duct Mach numbers for the remainder of the flow.
- (3) In this report, in order to extend the above design point analysis to other values of power setting, forward speed and altitude an overall effective nozzle area $A_e = 3604$ sq. in. has been used which applies since we have assumed that central and peripheral nozzles exhaust at the same pressure ratio. This procedure then provides a quick but slightly approximate answer (see Section 5.1).

TABLE II

Effect of forward speed on engine performance conditions.

Three Continental J69 engines at 22,700 rpm (max. power)
Altitude - Sea Level

Overall effective nozzle area $A_e = 3604$ sq. in.

Average exhaust gas temperature = 3880K

Mach Number	0	0.1	0.2	0.3	0.4
Flight speed V ft./sec.	0	111.7	223	335	447
Ram pressure rise P_1/p_a	1.0	1.0072	1.0283	1.0644	1.1167
Intake pressure recovery P_2/P_1	1.0	0.9995	0.9975	0.99	0.97
Fan pressure ratio P_3/P_2	1.0996	1.0996	1.0996	1.0996	1.0996
Duct pressure loss P_6/P_3	0.9666	0.9666	0.9666	0.9666	0.9666
Nozzle pressure ratio p_a/P_6	0.9408	0.9346	0.9173	0.8928	0.8686
Thrust function $F_G/A_6 p_6$	0.1227	0.1366	0.1755	0.23	0.2889
Mass flow function $Q/\sqrt{T_6/A_6 p_6}$	0.2045	0.216	0.2455	0.2822	0.3175
Mass flow Q lb.	550	580.9	660.2	758.9	853.78
Gross thrust F_G lb.	6500	7,235	9,295	12,186	15,304
0.9 F_G	—	6,512	8,366	10,967	13,774
Momentum drag QV/g lb.	0	2015	4572	7895	11852
Net thrust F_n lb.	6500	4497	3794	3073	1922
F_n/p_a	3.072	2.125	1.793	1.452	0.908
W_f/p_6	1.474	1.474	1.474	1.474	1.474
W_f/p_a	1.567	1.577	1.607	1.651	1.697

565 77 895 114

$Q, F_0 p_6$
 I_0

SECRET

9.0 (continued)

TABLE III

Effect of reduction in power setting on engine performance conditions:

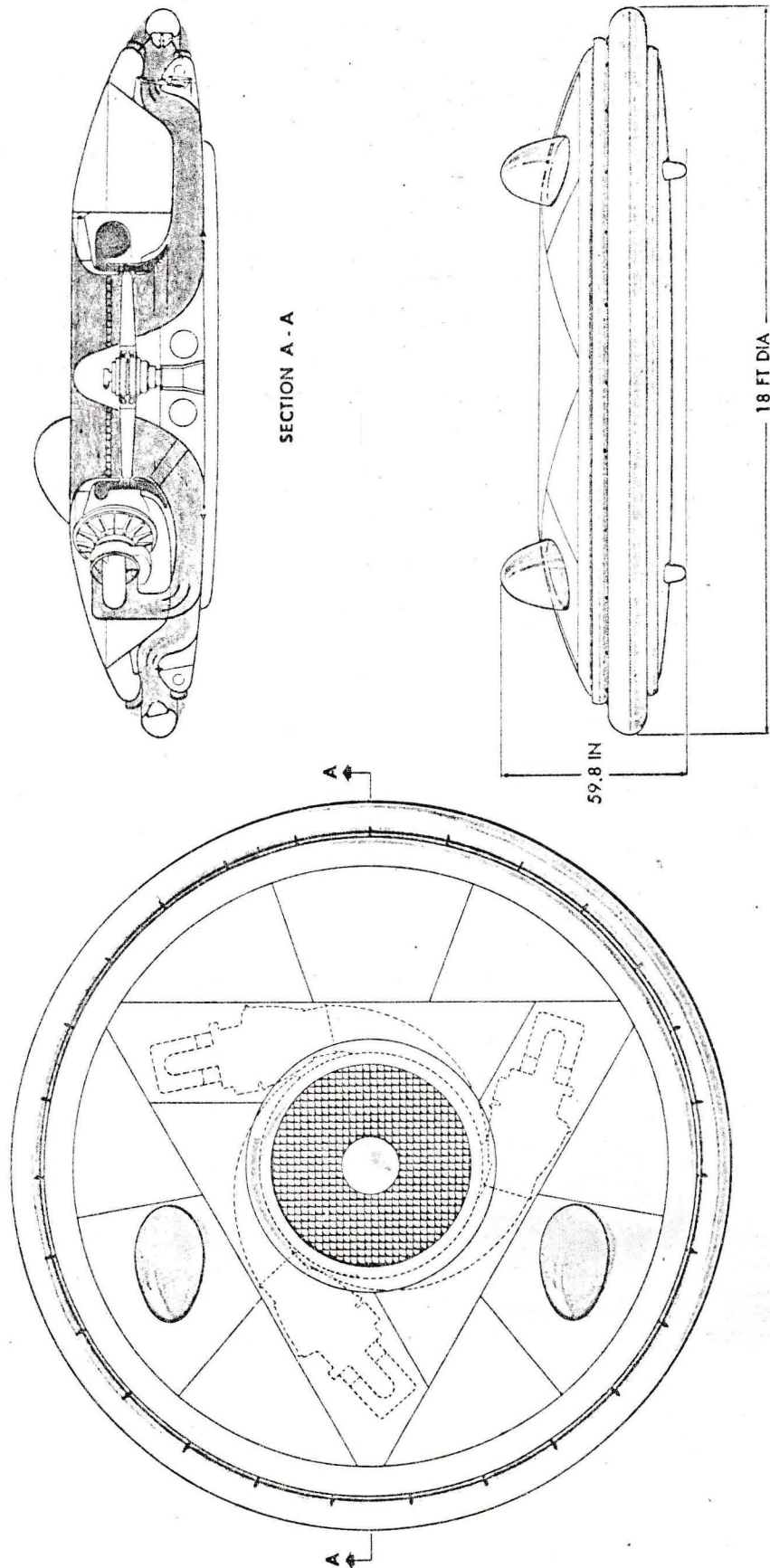
3 J69 engines operative
Sea Level I.S.A. condition
Zero forward speed

J69 Engine Speed	22,700	21,000	19,150
Fan pressure ratio P_3/P_2	1.0997	1.0780	1.0578
Duct loss P_6/P_3	.9666	.9737	.9804
Average exhaust temp. °K	388	388	388
Gross thrust	6500	5136	3906
Fuel flow W_f/p_6	1.474	1.125	0.875

10.0 LIST OF ILLUSTRATIONS

- Fig. 1 General Arrangement
- Fig. 2 Engine Installation
- Fig. 3 Structure Cutaway
- Fig. 4 Turborotor Assembly
- Fig. 5 Flow Distribution - Hovering and Ground Cushion
- Fig. 6 Intake Pressure Recovery
- Fig. 7 Fuel Flow
- Fig. 8 Lift versus Drag
- Fig. 9 C_D versus CL^2
- Fig. 10 Thrust Augmentation in the Ground Cushion
- Fig. 11 Payload in the Ground Cushion
- Fig. 12 Hovering Endurance in the Ground Cushion
- Fig. 13 Thrust and Drag in Forward Flight
- Fig. 14 Maximum Speed versus Altitude.
- Fig. 15 Specific Air Range at S.L.
- Fig. 16 Specific Air Range at 10,000 ft.
- Fig. 17 Rate of Climb versus Altitude.
- Fig. 18 Time to Height
- Fig. 19 Speed versus Range
- Fig. 20 Payload versus Range
- Fig. 21 Schematic of Gyro Damping System
- Fig. 22 Control Nozzle Mechanism
- Fig. 23 Response Curves
- Fig. 24 Response Curves

SECRET

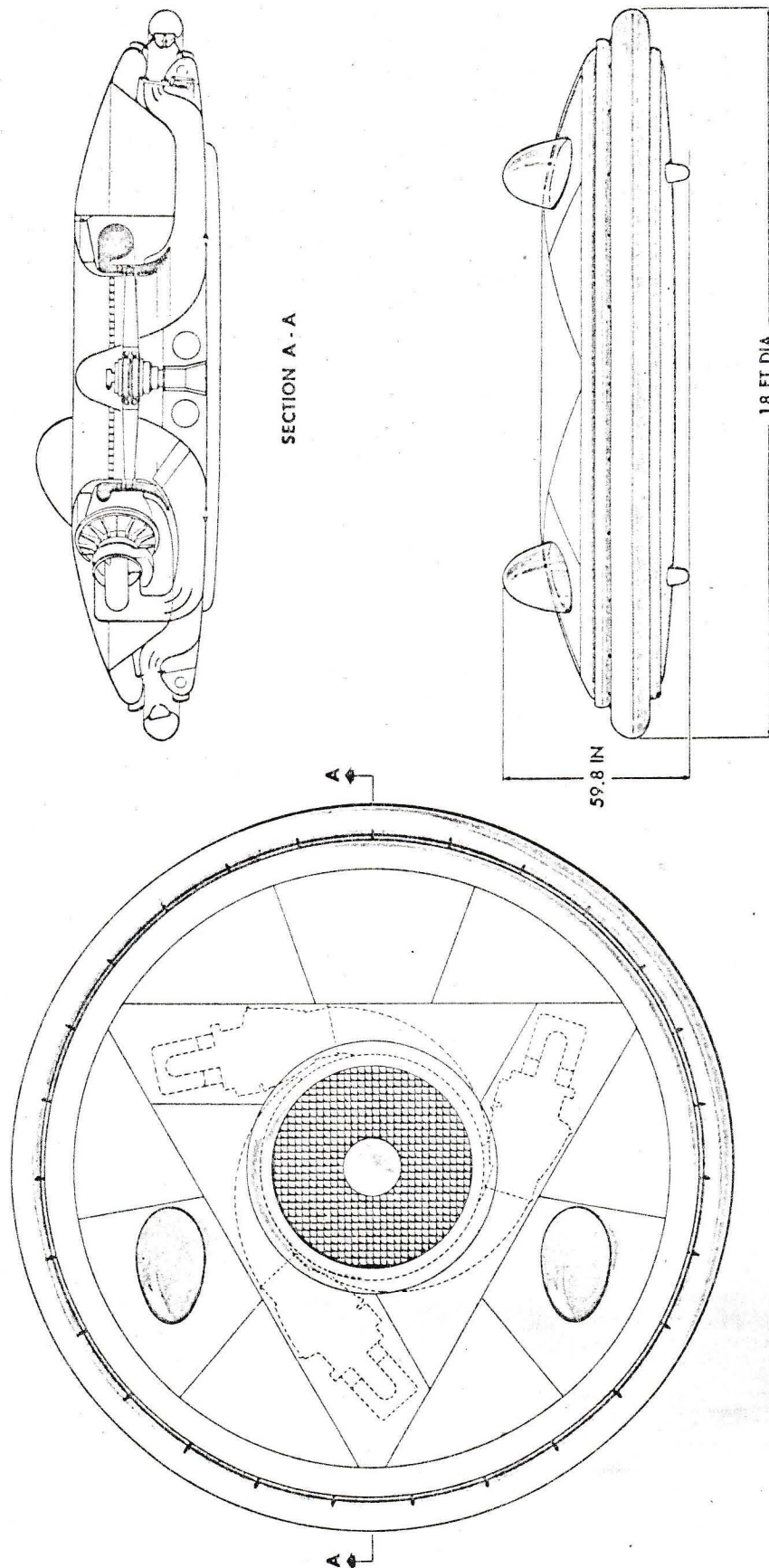


3419-802-2

FIG 1 3 VIEW GENERAL ARRANGEMENT OF AVROCAR 1

SECRET

SECRET



3419-602-2

FIG 1 3 VIEW GENERAL ARRANGEMENT OF AVROCAR 1

SECRET

SECRET

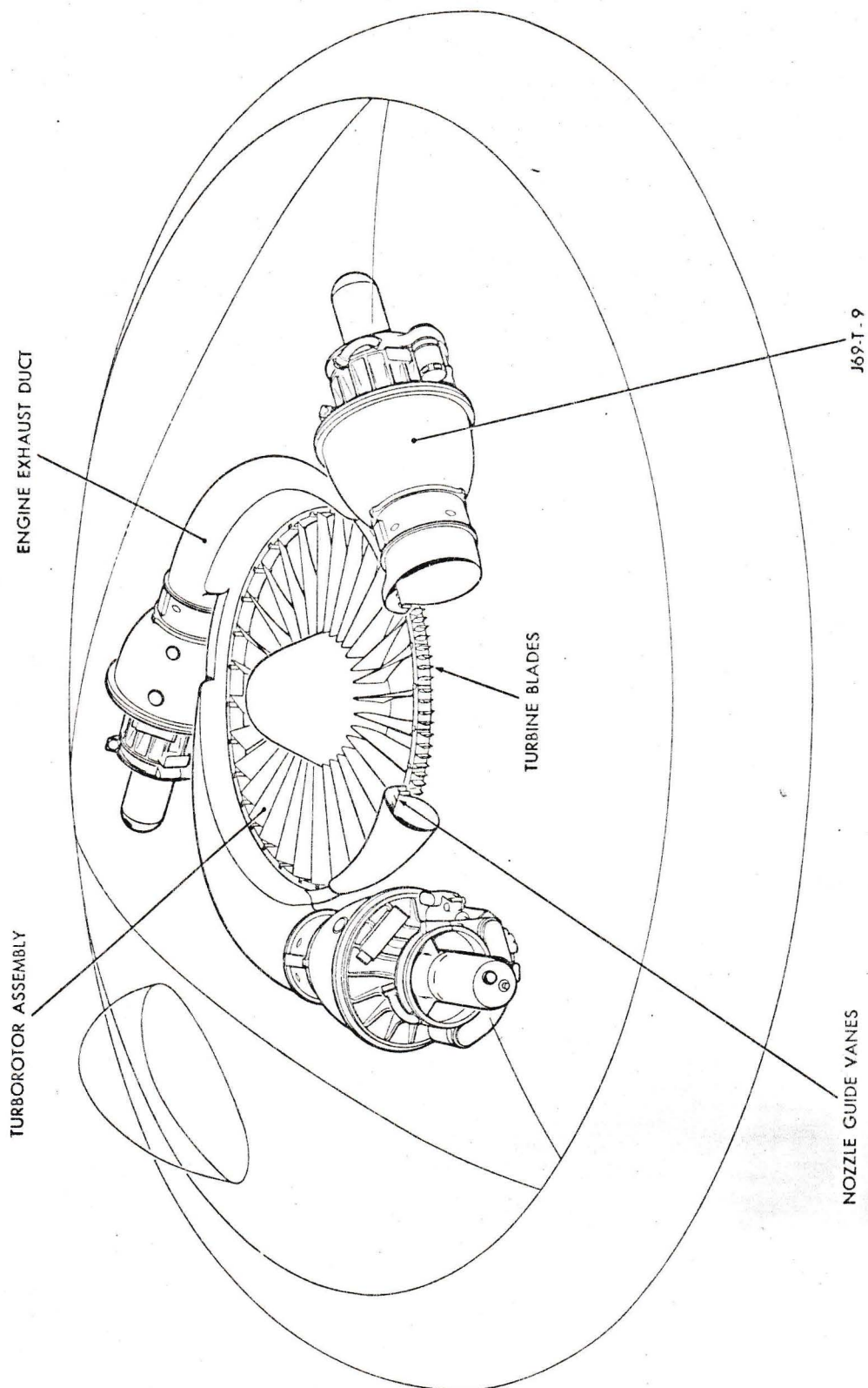


FIG. 2 ENGINE INSTALLATION

SECRET

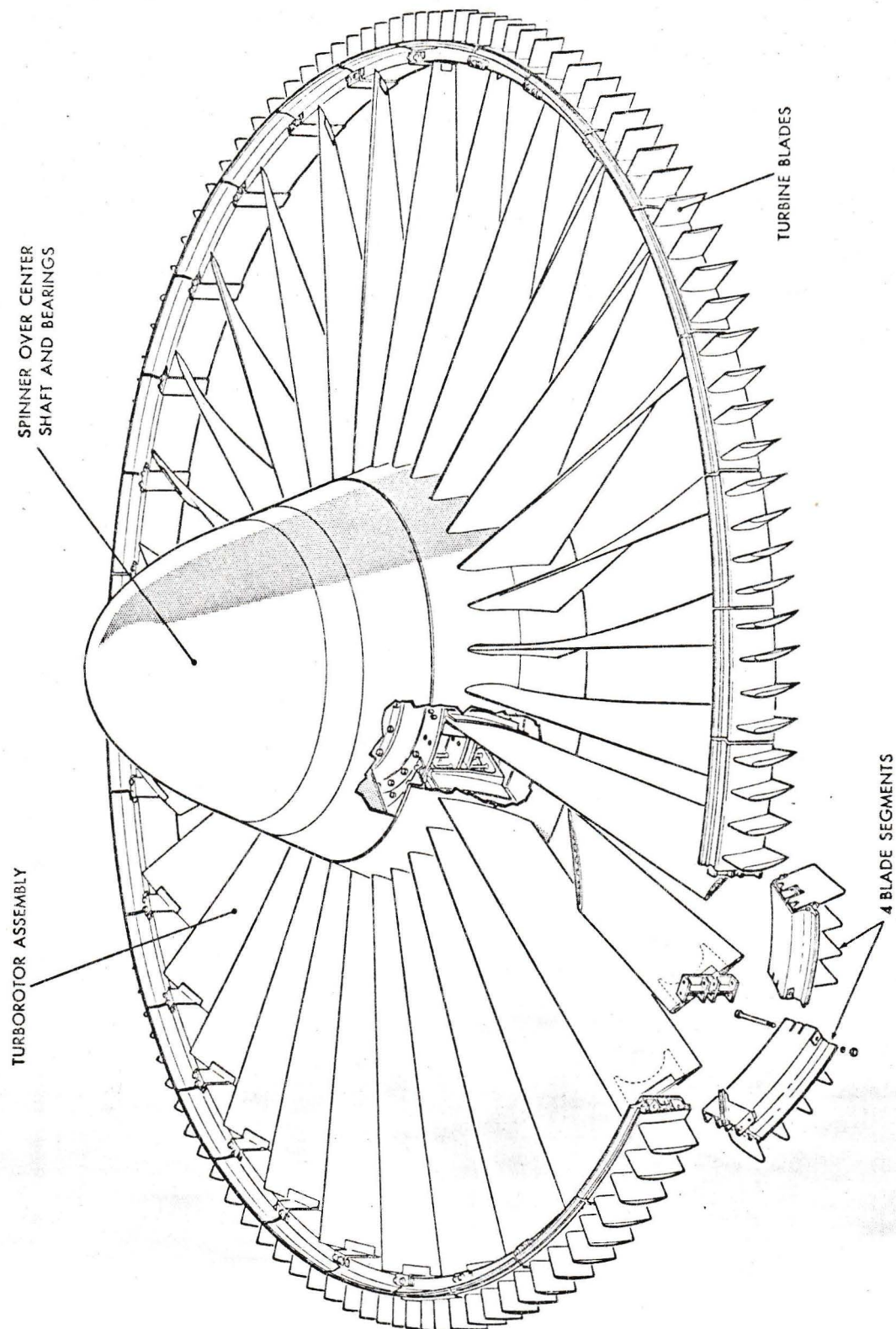
SECRET

FIG. 3 TURBOROTOR ASSEMBLY

SECRET

SECRET

AVRO/SPG/TR 174

3390-002-1

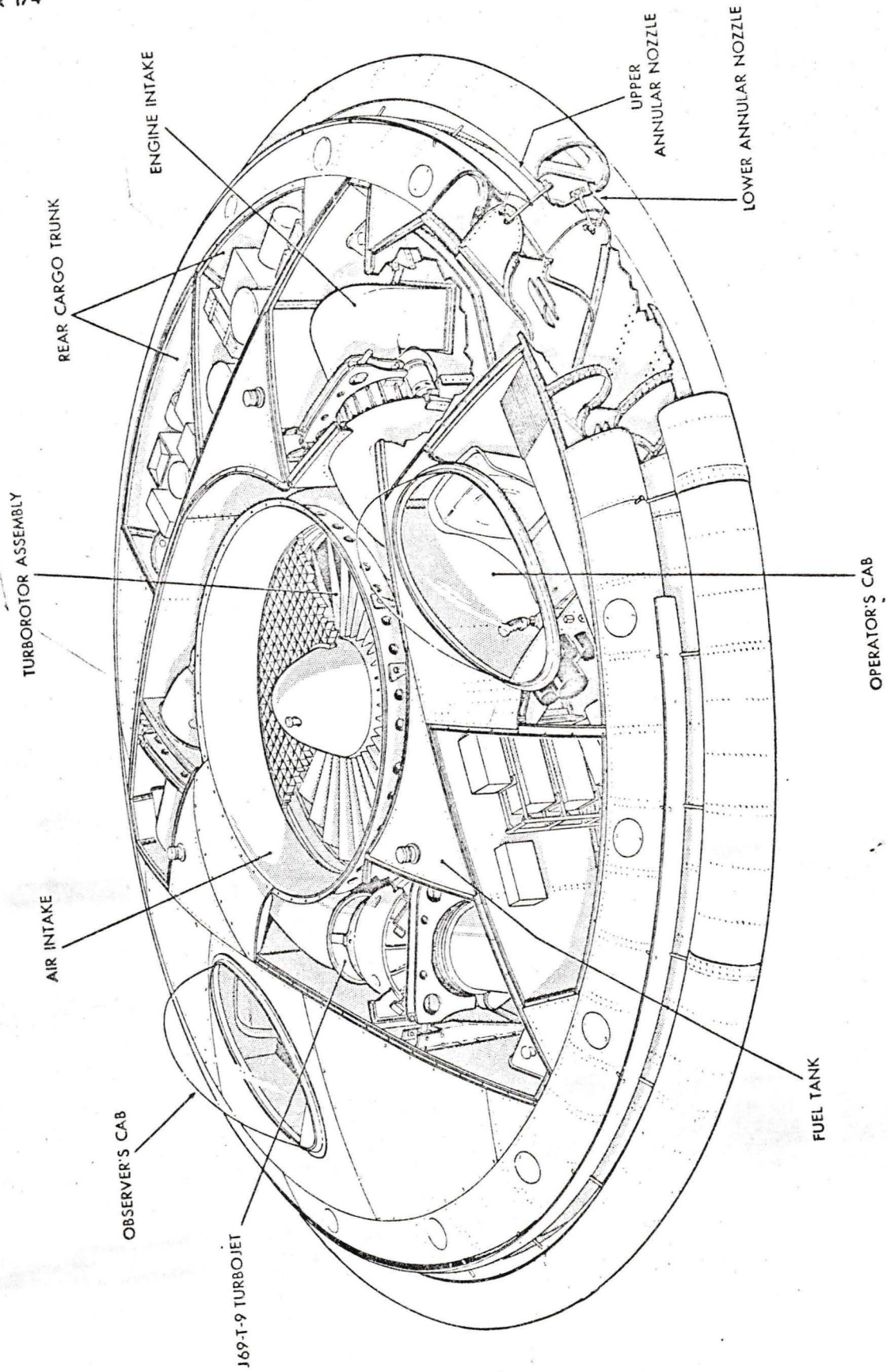
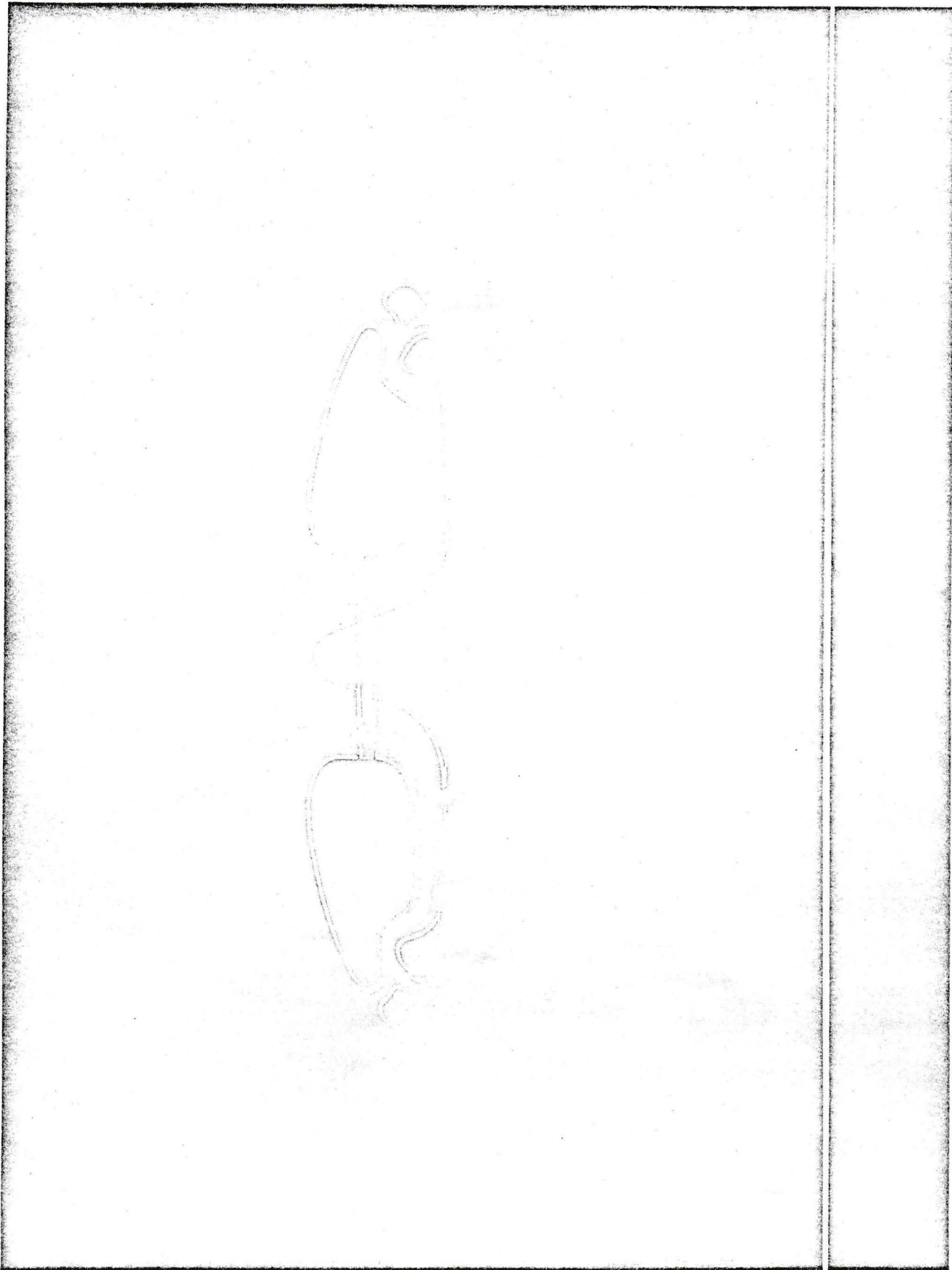


FIG. 4 STRUCTURE CUTAWAY

SECRET

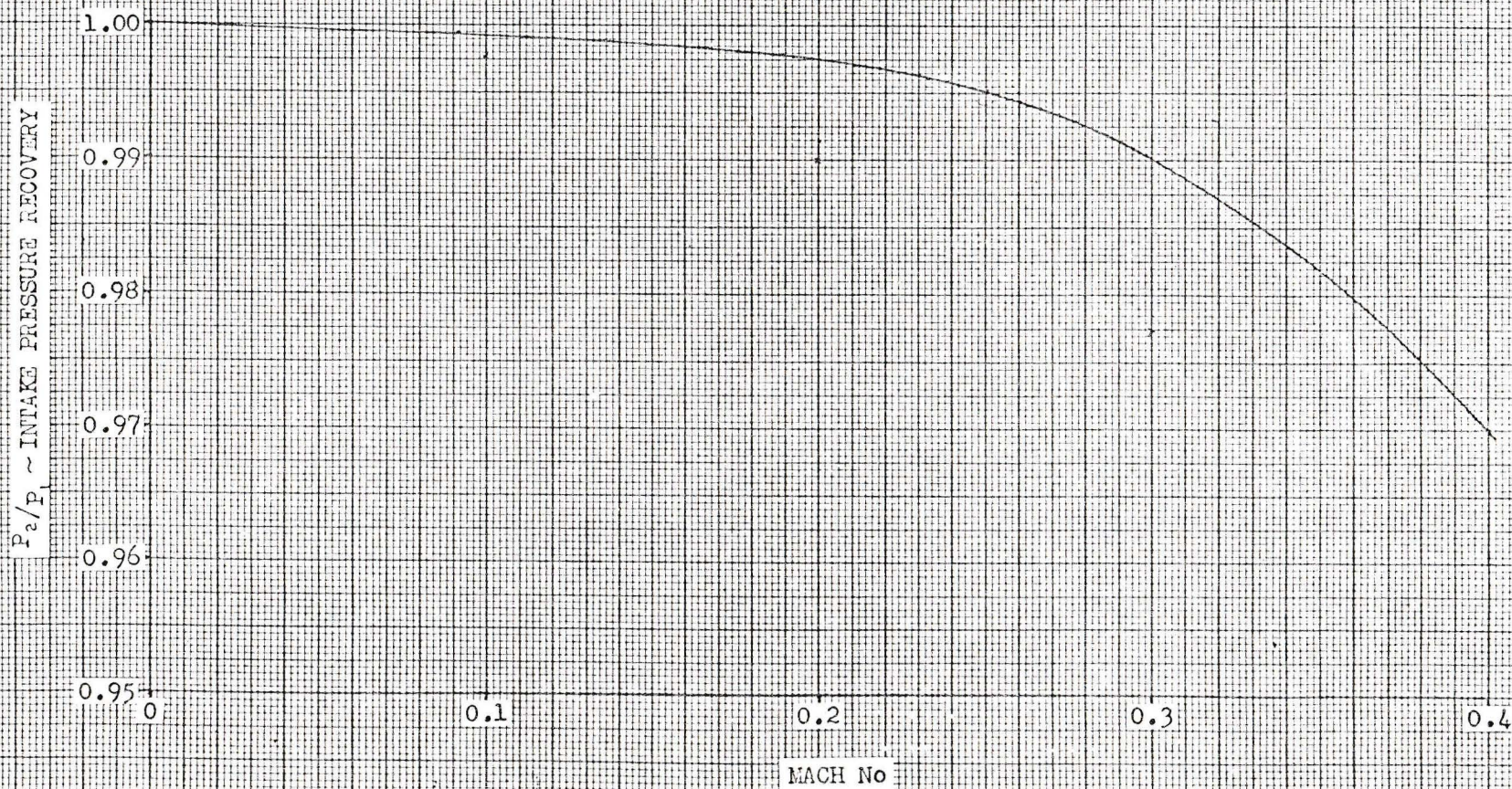


3396-002-2

FIG. 5 FLOW DISTRIBUTION - HOVERING

SECRET

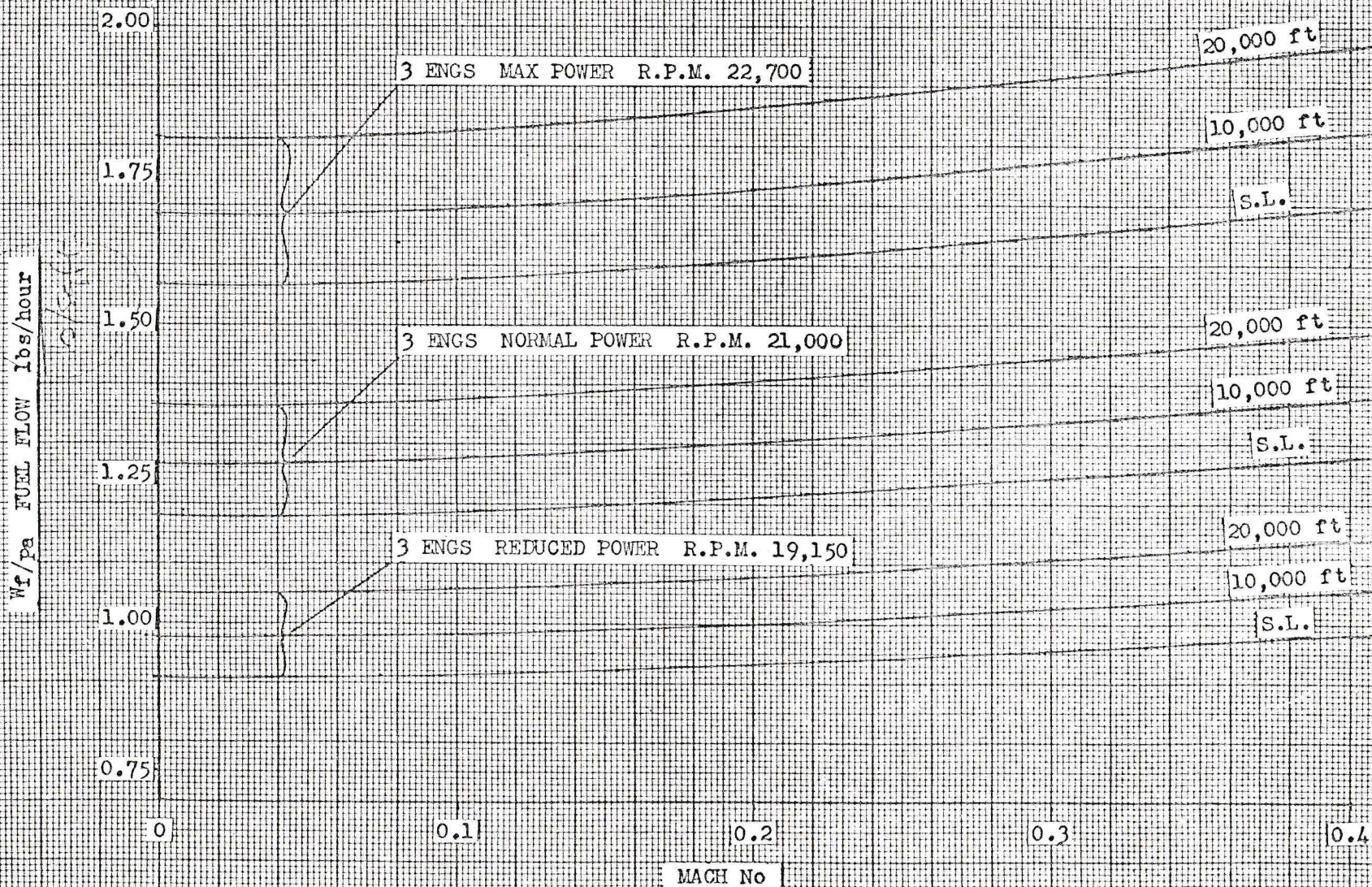
FIG 6. INTAKE PRESSURE RECOVERY VERSUS MACH No



SECRET

SECRET

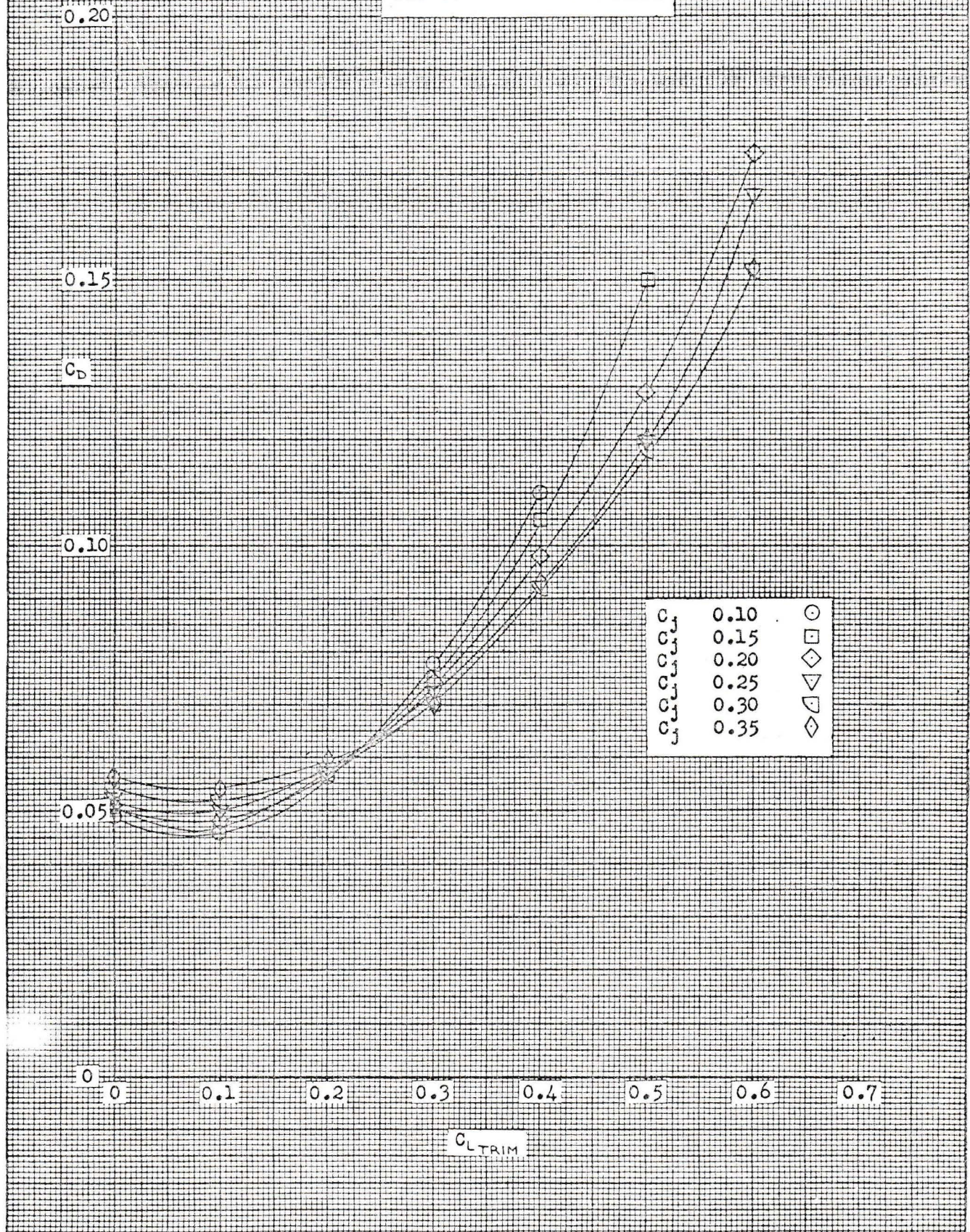
FIG 7. POWERPLANT FUEL FLOW

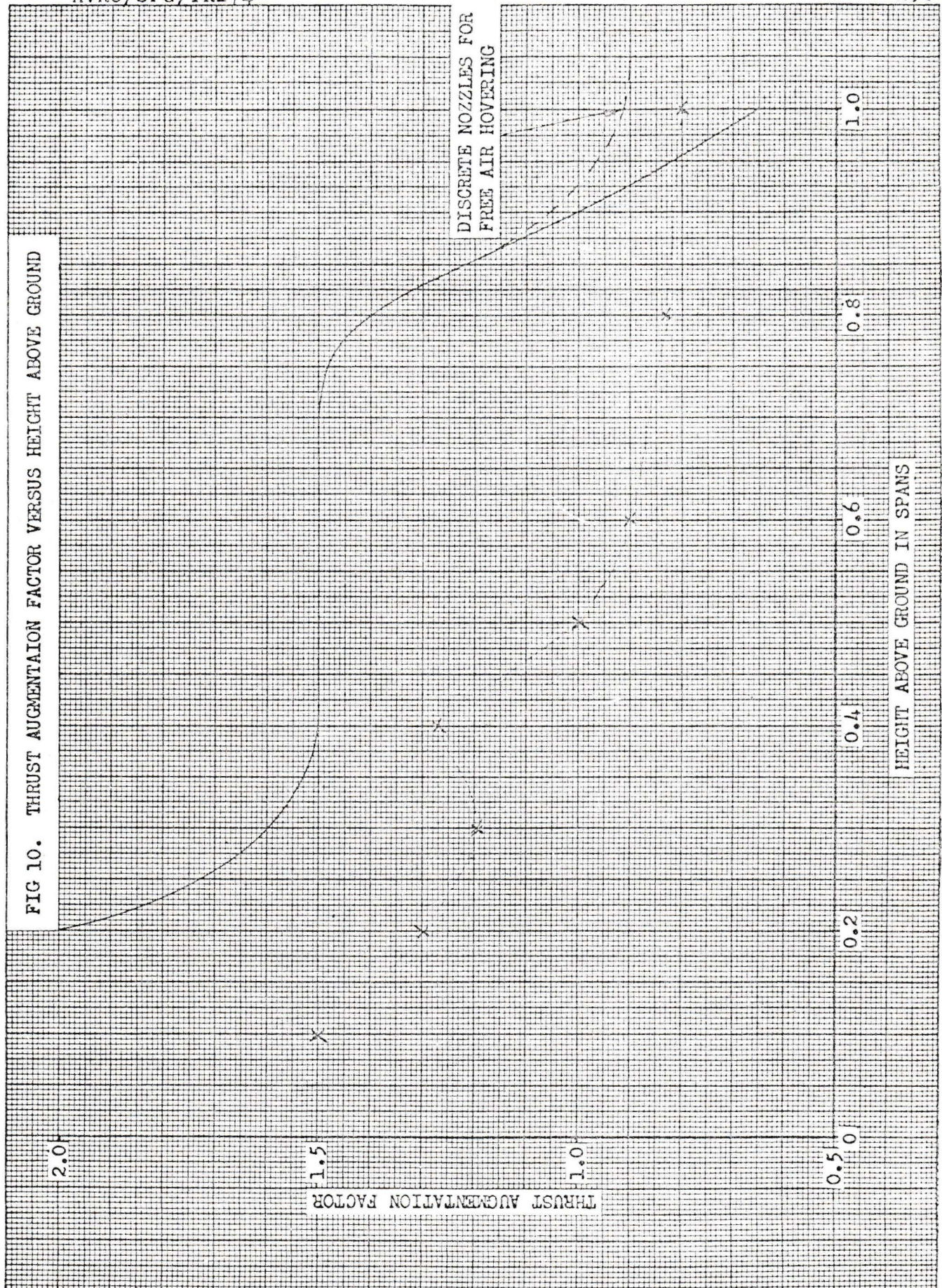


AVRO/S.P.G./TR 174

SECRET

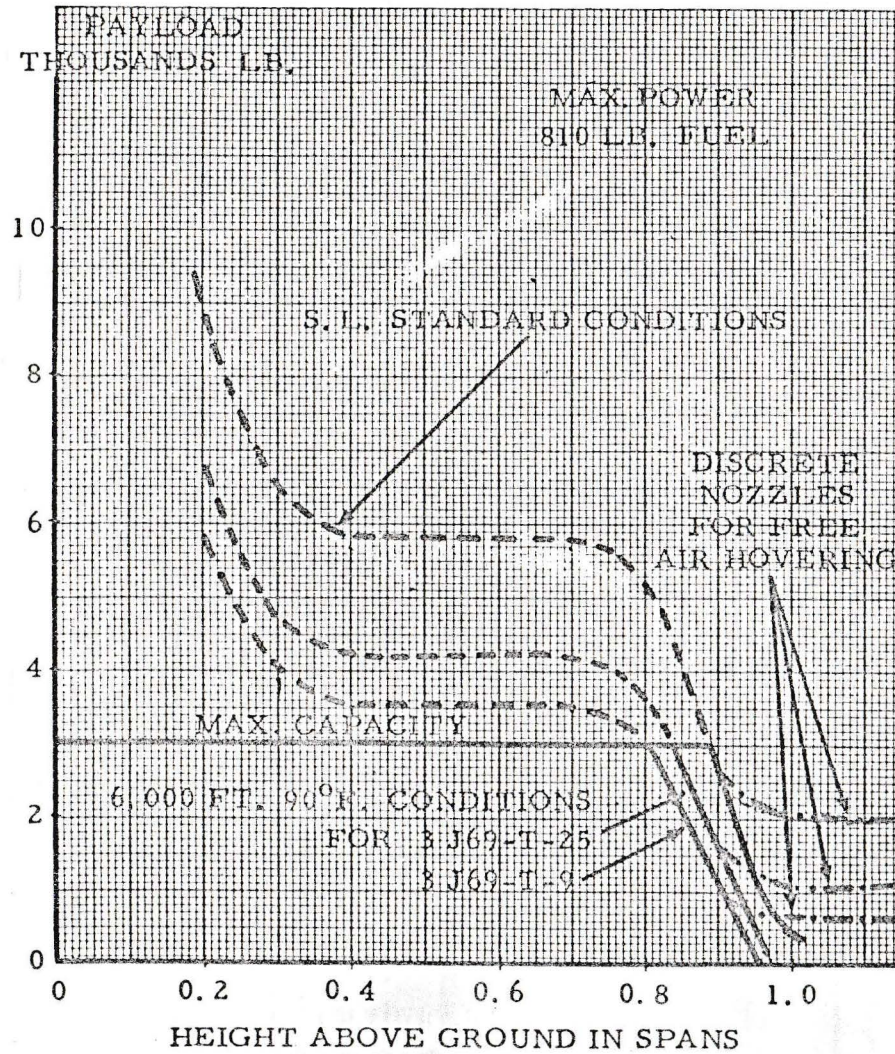
FIG 8. DRAG COEFFICIENT





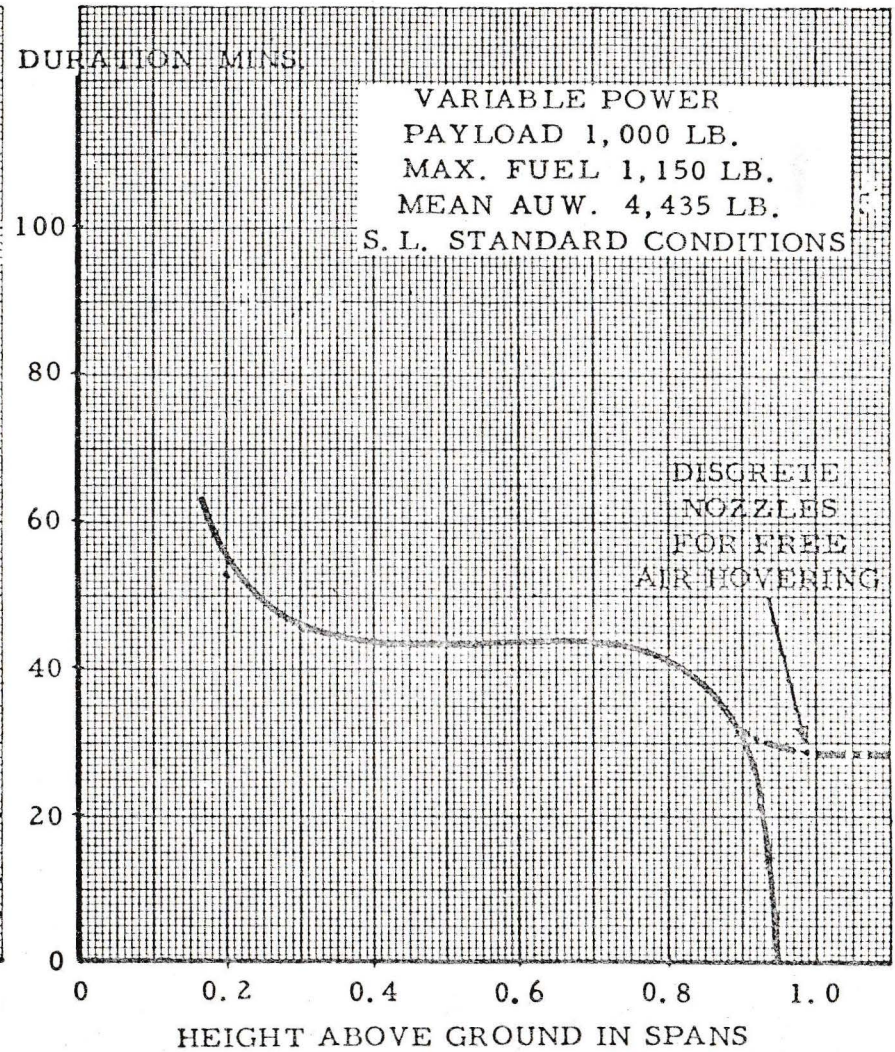
SECRET

AVROCAR 3 CONTINENTAL J69-T-9 ENGINES ESTIMATED HOVERING PERFORMANCE



STATIC LIFTING PERFORMANCE

FIG. 11

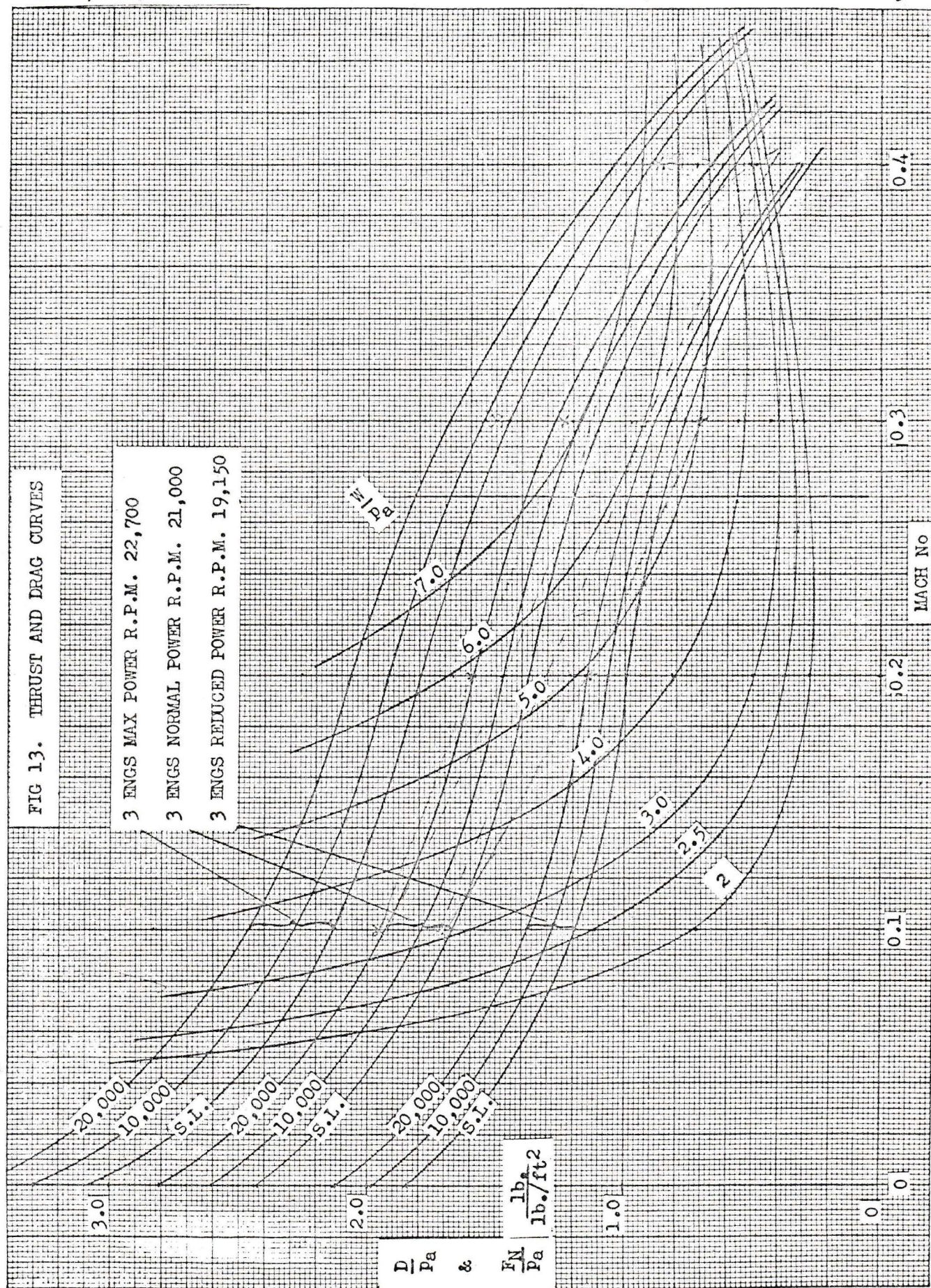


HOVERING ENDURANCE

FIG. 12

AVRO/SPC/TR174

SECRET



SECRET

FIG. 14.

ALTITUDE FT.

AVROCAR 3 CONTINENTAL J-69-T-9 ENGINES
ESTIMATED MAXIMUM SPEEDS VERSUS ALTITUDE

J.69 ENGINE SPEED 22700 RPM

A/C WT. LB.

4000
6000
8000

TRUE AIRSPEED KNOTS

AVRO/SPG/TRJ74

SECRET

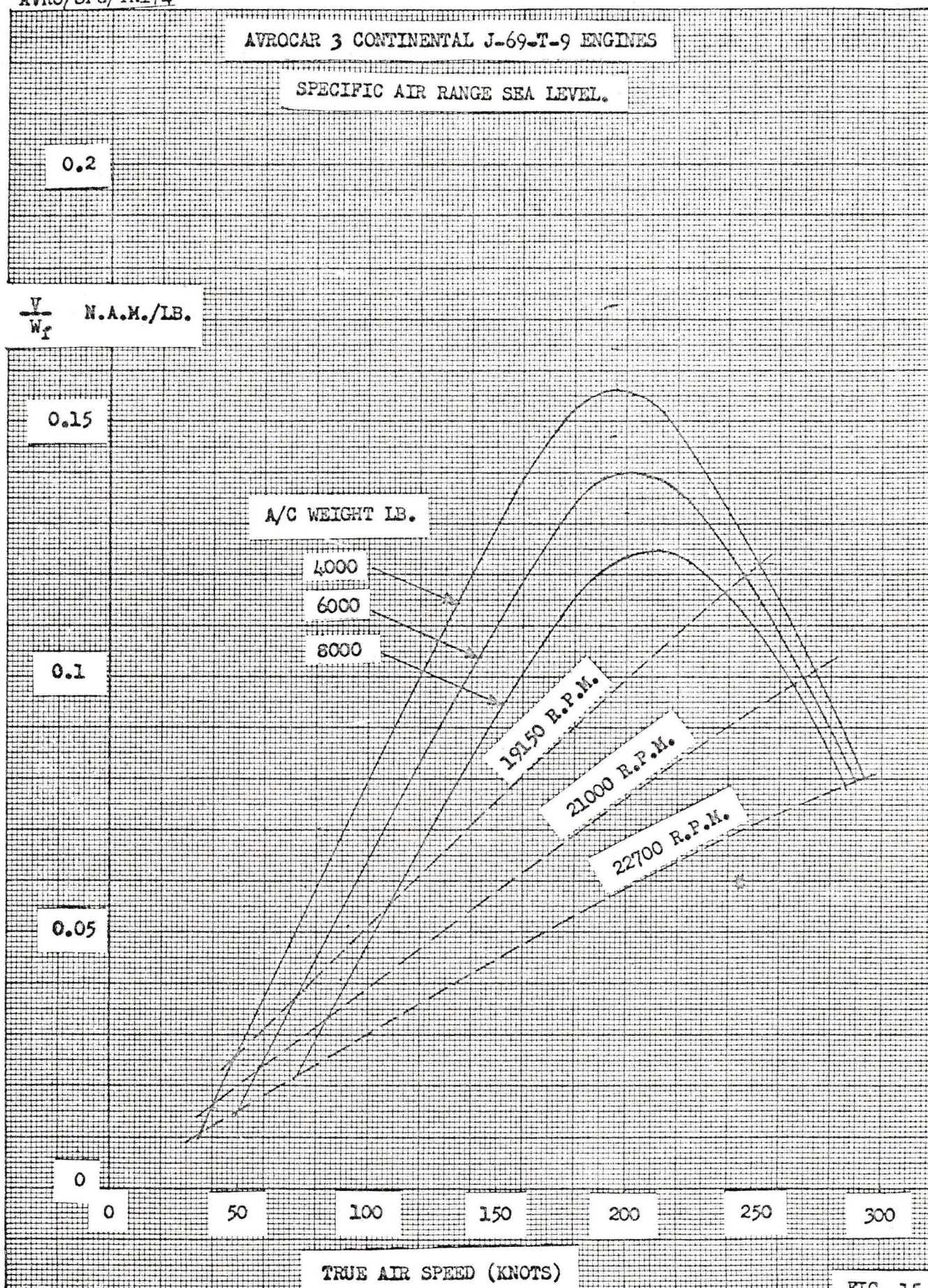


FIG. 15

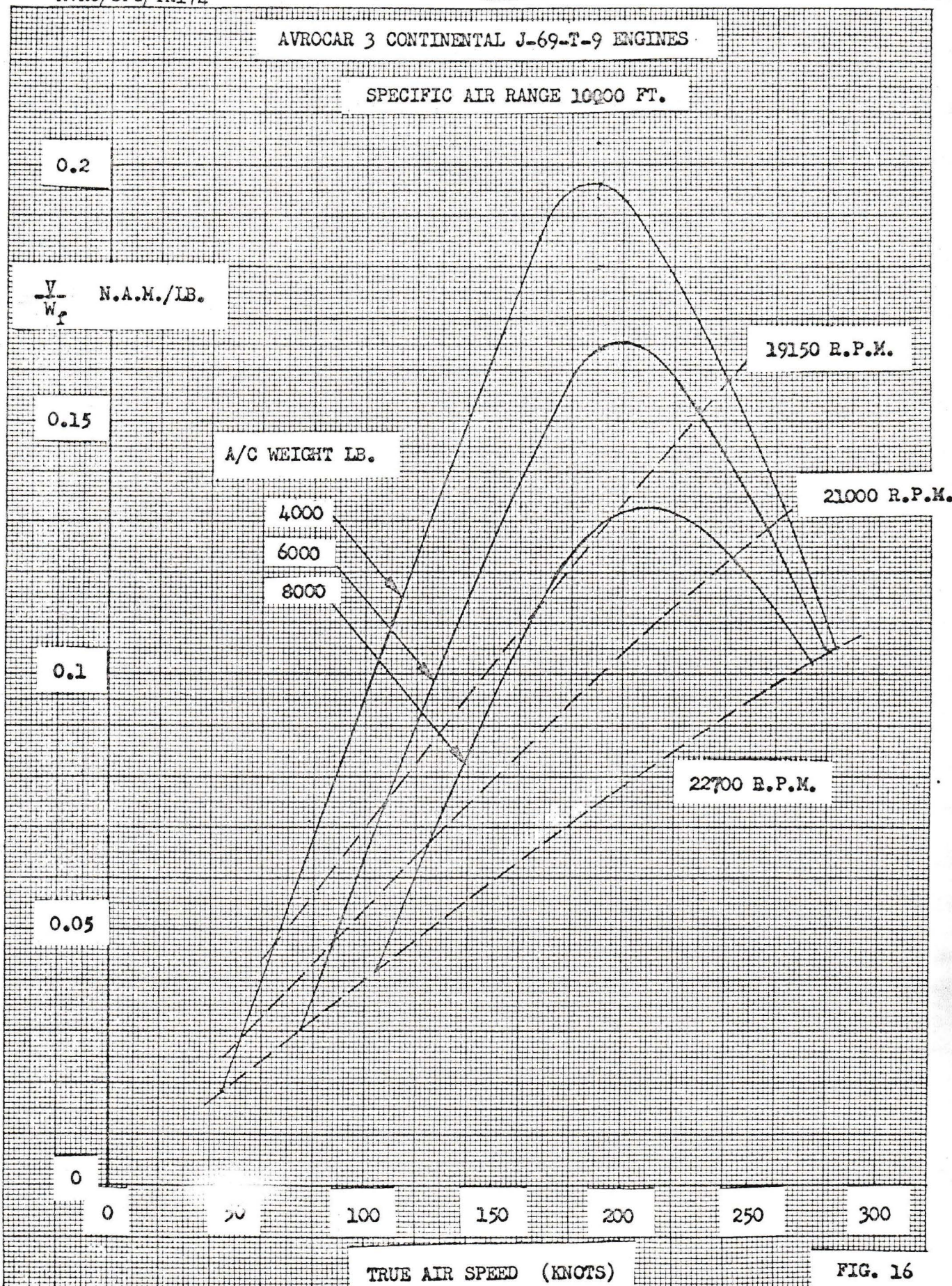


FIG. 16

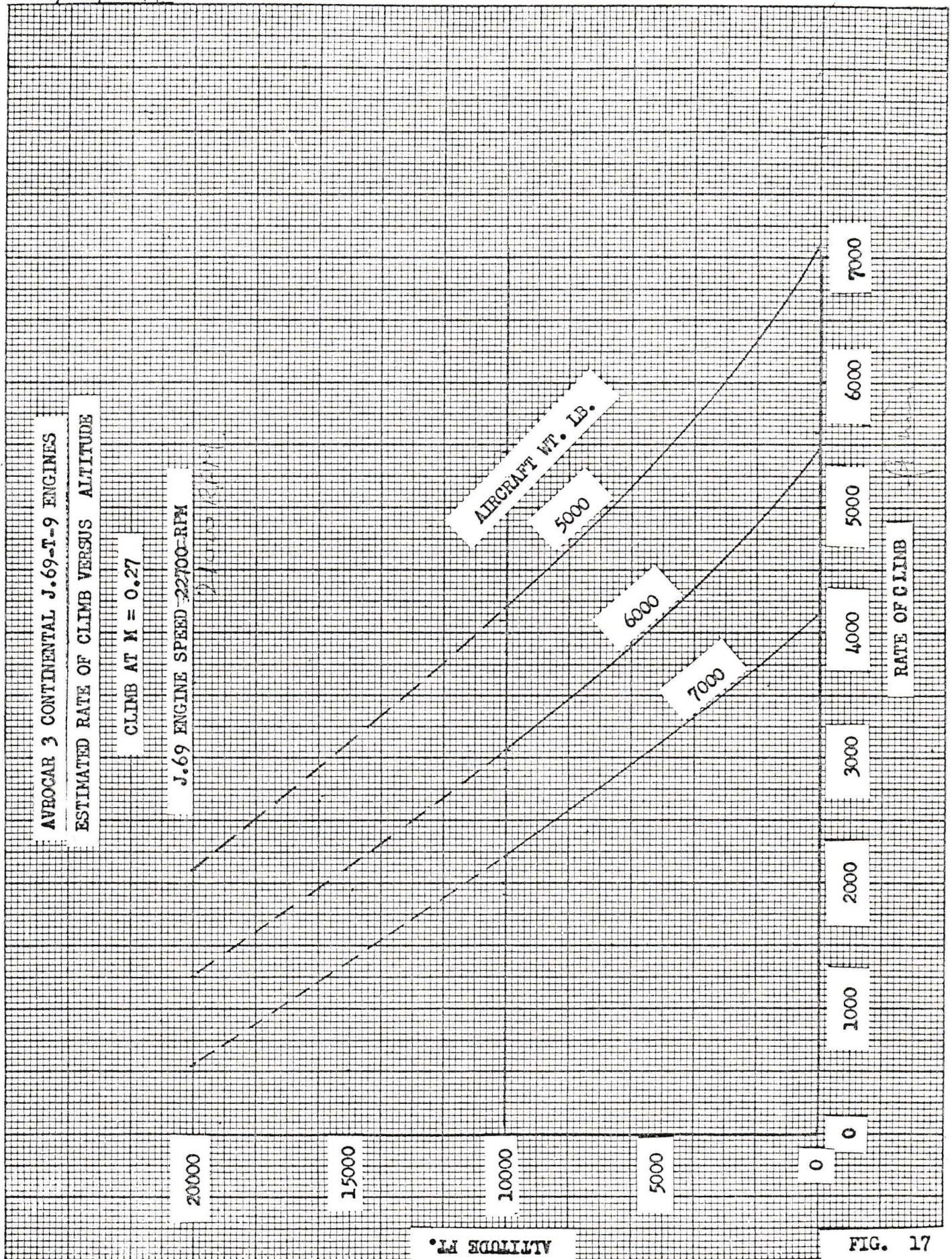


FIG. 17

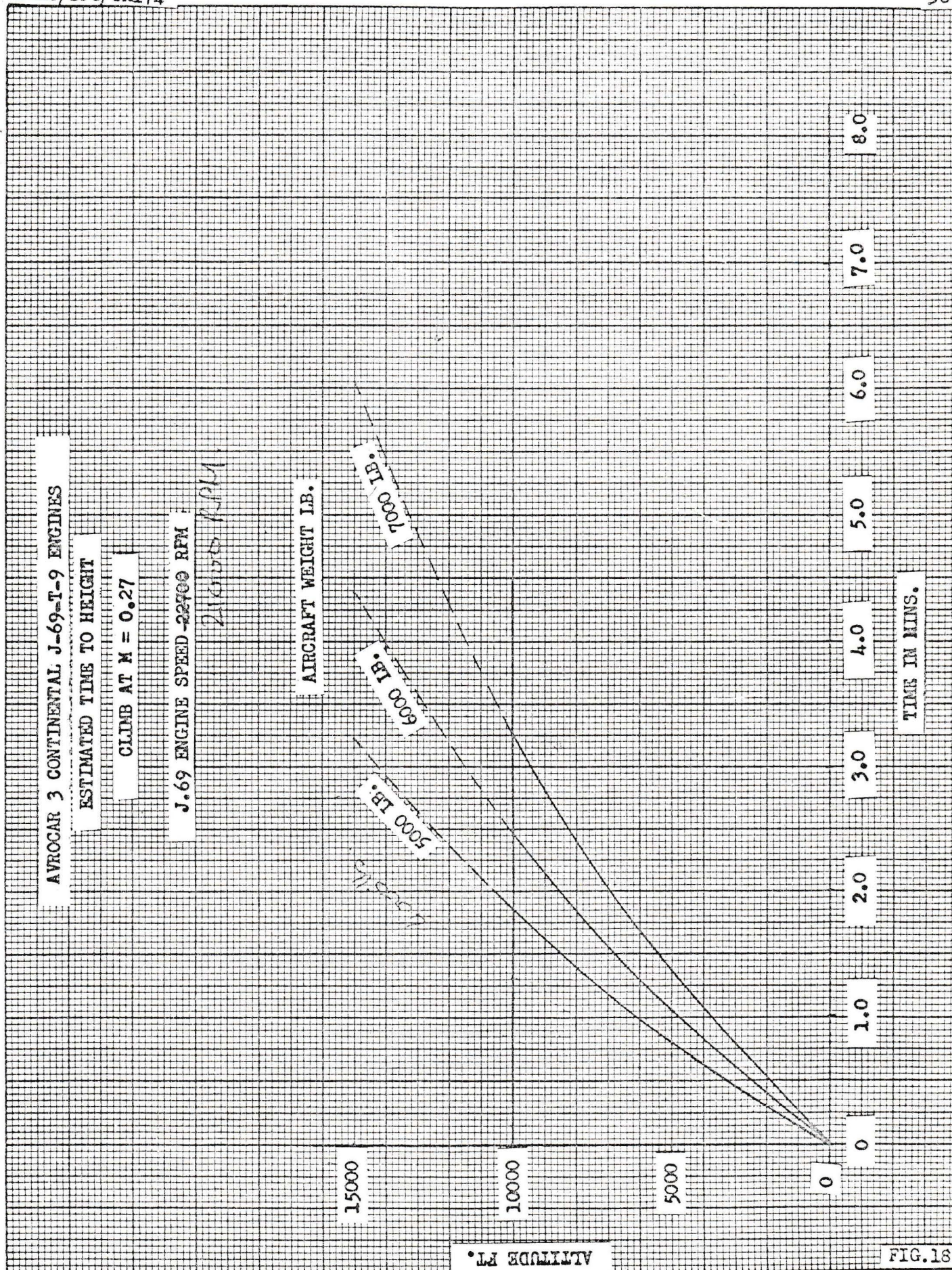


FIG. 18

TRUE AIRSPEED KNOTS

AVG. FOR CRUISE

AVROCAR 3 CONTINENTAL J-69-T-9 ENGINES

SPEED VERSUS RANGE (ESTIMATED)

250

200

150

100

0

0

50

100

150

200

250

V.T.O.

T.O.W. = 5650 lb.

PAYLOAD = 2020 lb.

FUEL = 810 lb.

S.L. CRUISE

GROUND CUSHION T.O.

T.O. W. = 6970 lb.

MAX PAYLOAD = 3000 lb.

MAX FUEL = 1150 lb.

(normal tanks)

S.L. CRUISE

V.T.O.

T.O.W. = 4200 lb.

MIN PAYLOAD = 250 lb.

MAX FUEL = 1150 lb.

(normal tanks)

10000 ft CRUISE

RANGE N.A.M.

AVROCAR 3 CONTINENTAL J.69-T-9 ENGINES

PAYLOAD VERSUS RANGE (ESTIMATED)

S.L. STANDARD CONDITIONS

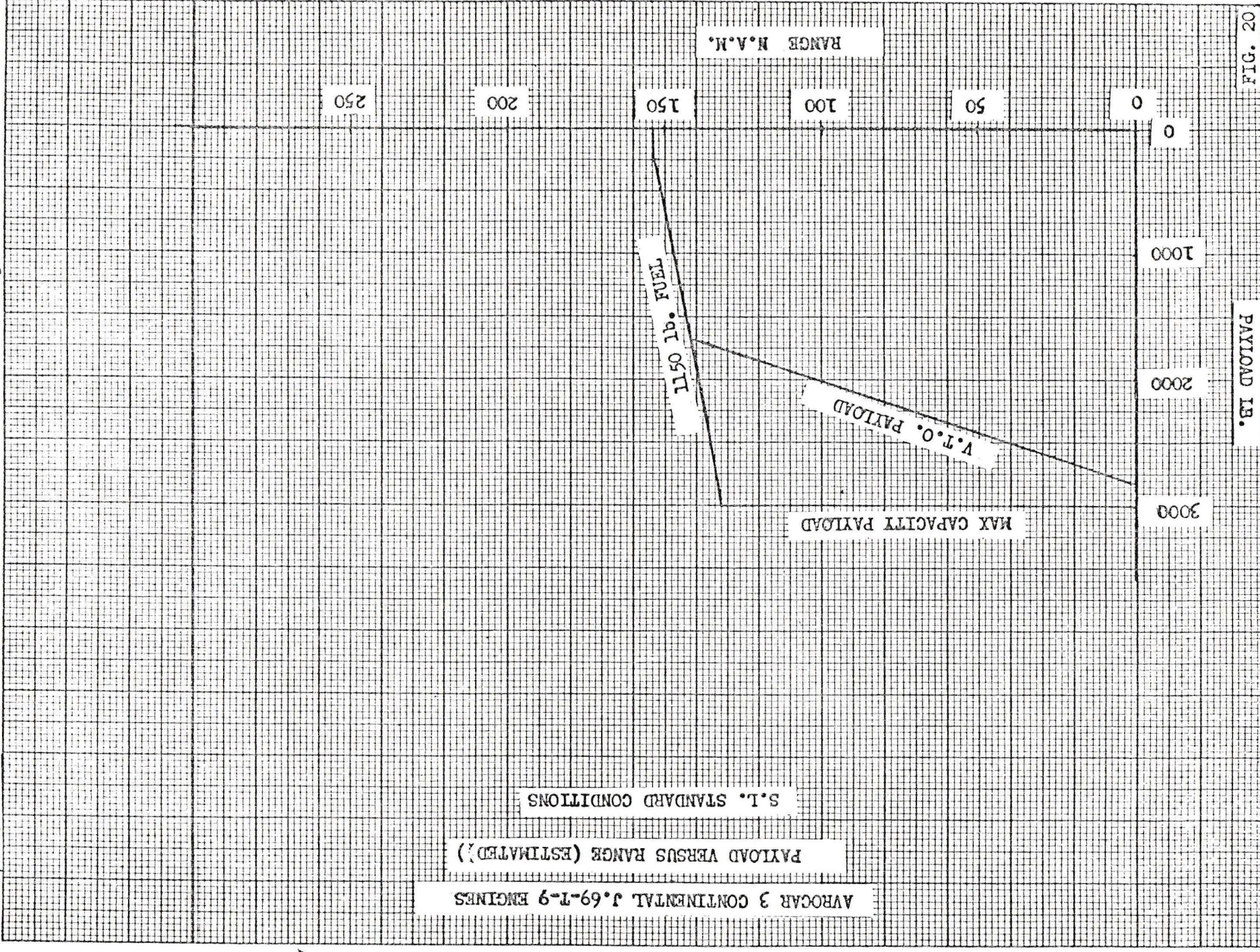


FIG. 20

PAYLOAD LB.

RANGE N.A.M.

3466-802-1

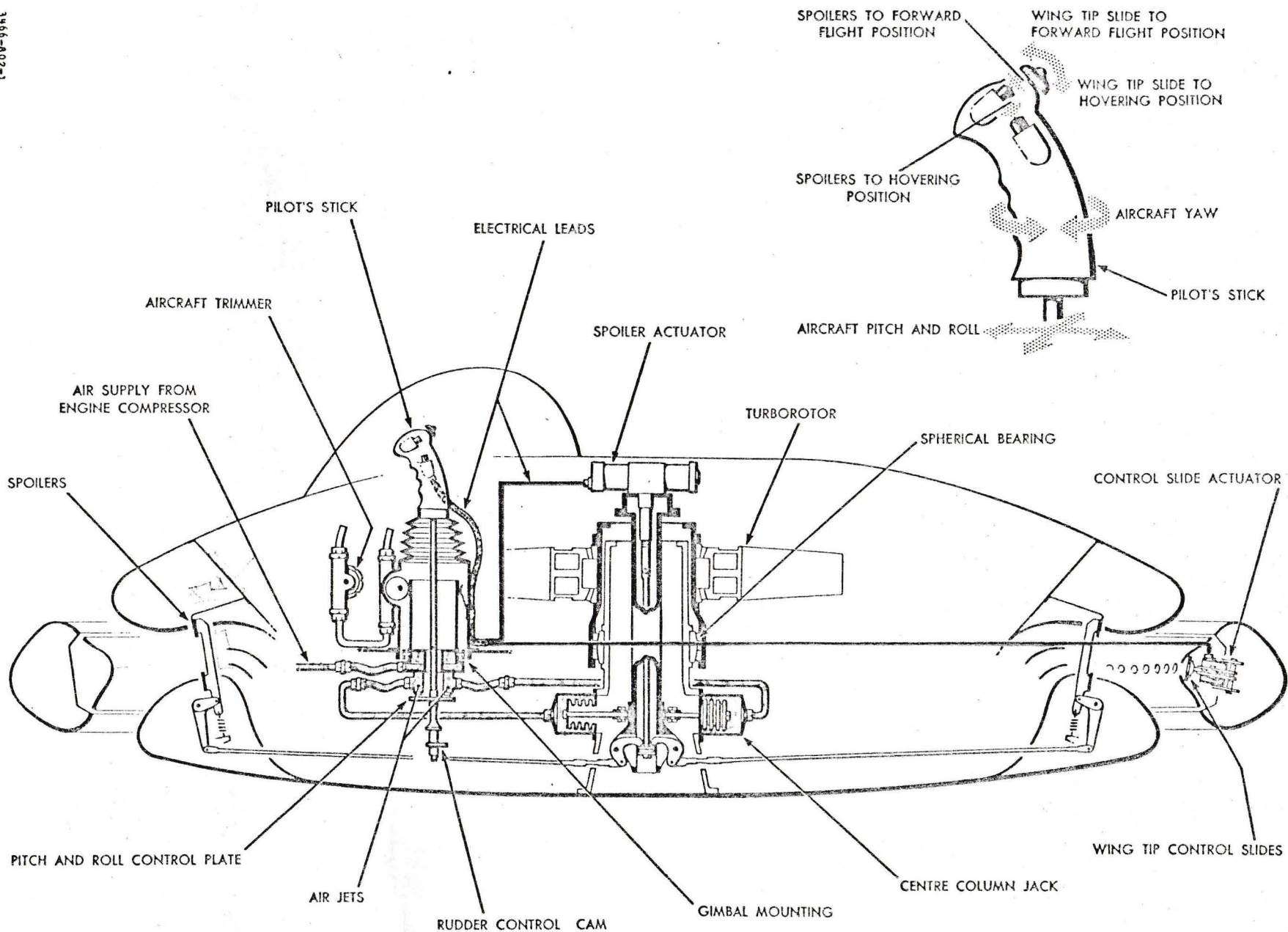


FIG. 21 GYRO DAMPING SYSTEM

SECRET

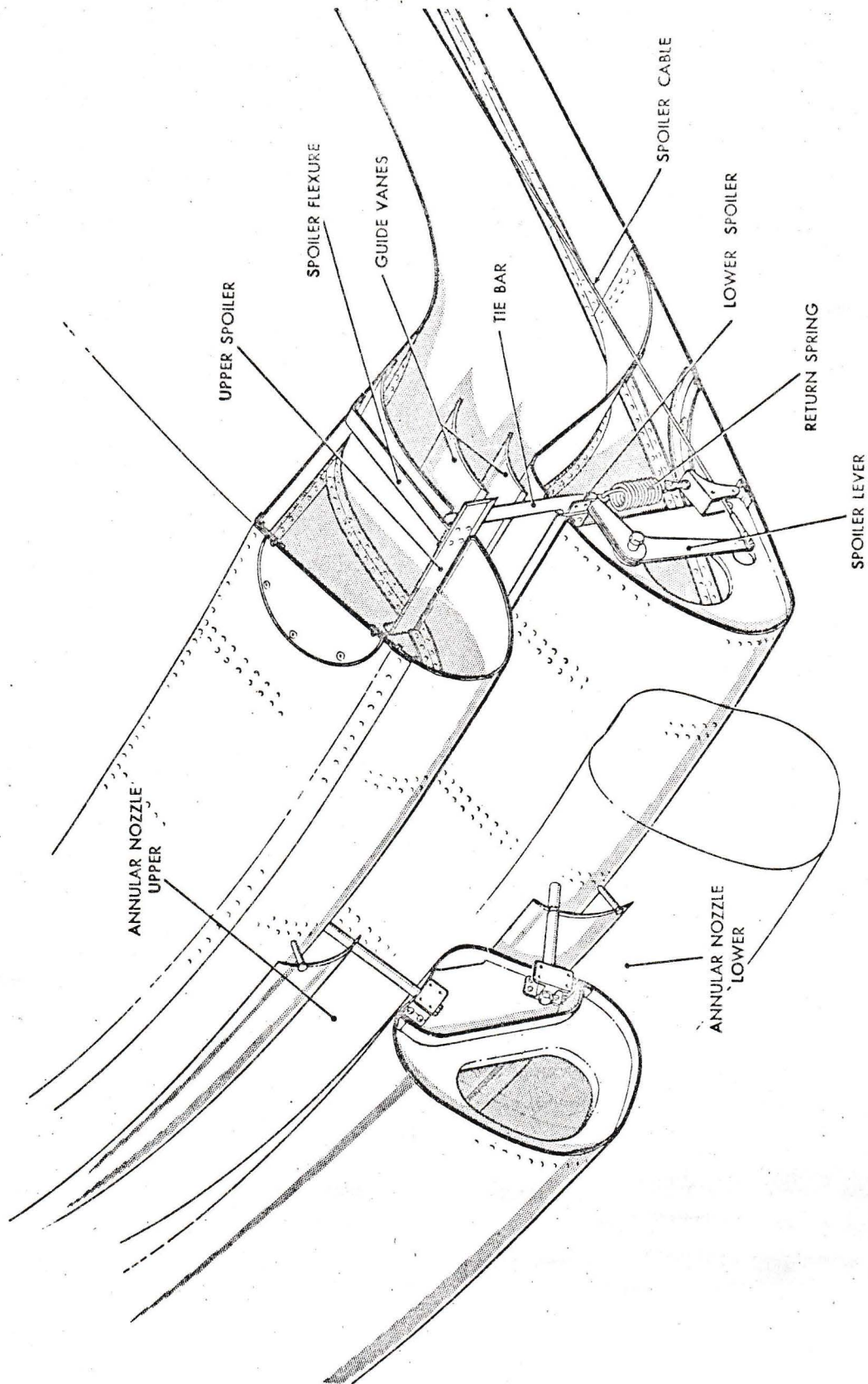
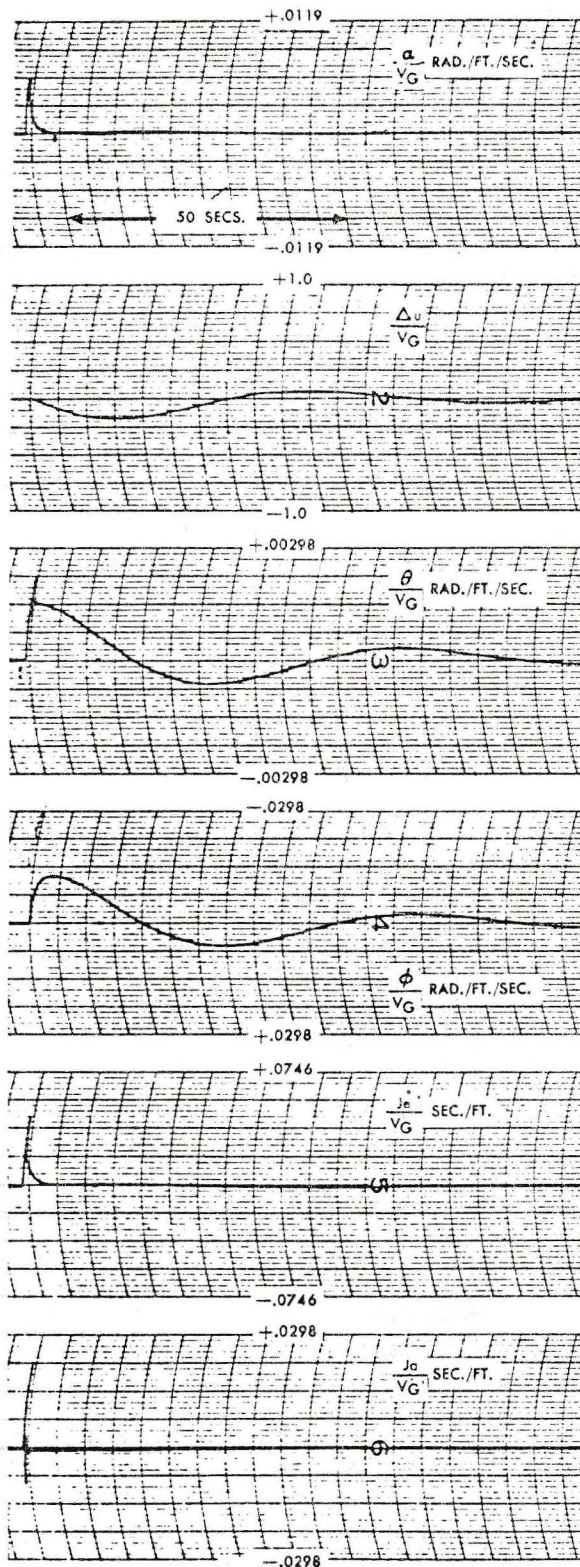
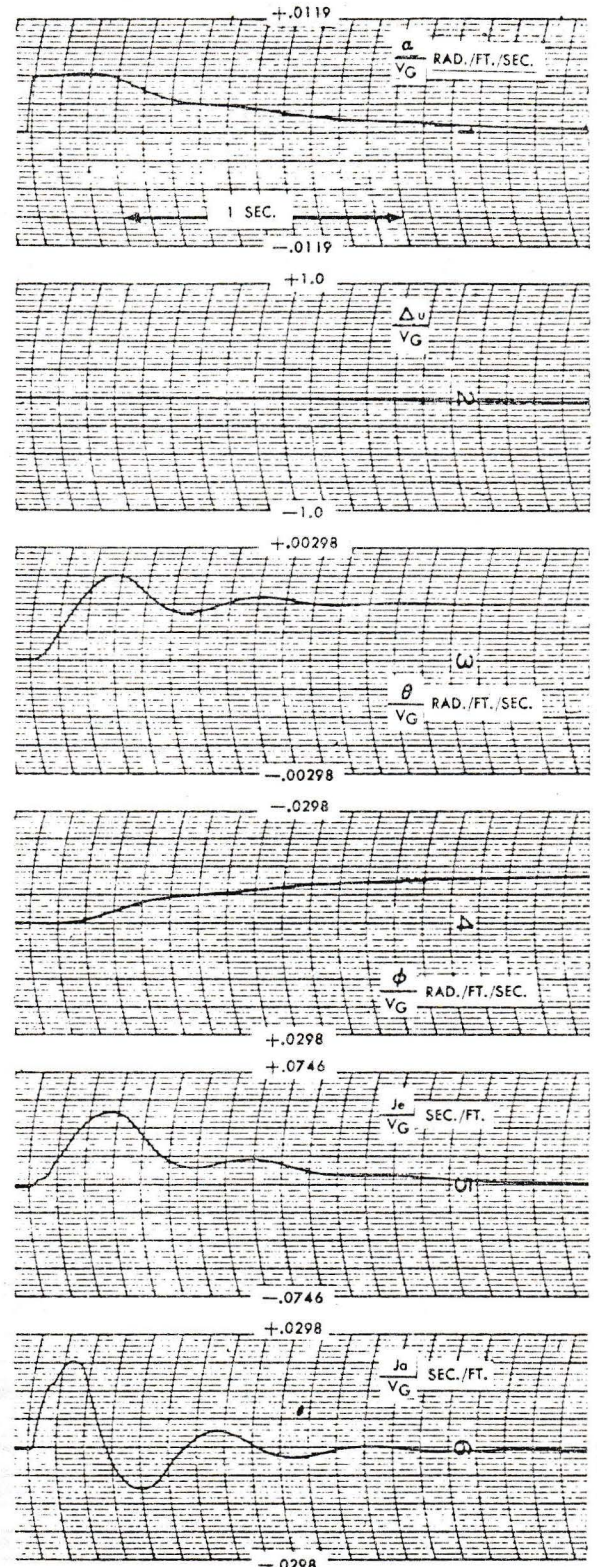
SECRET

FIG. 22 CONTROL NOZZLE MECHANISM

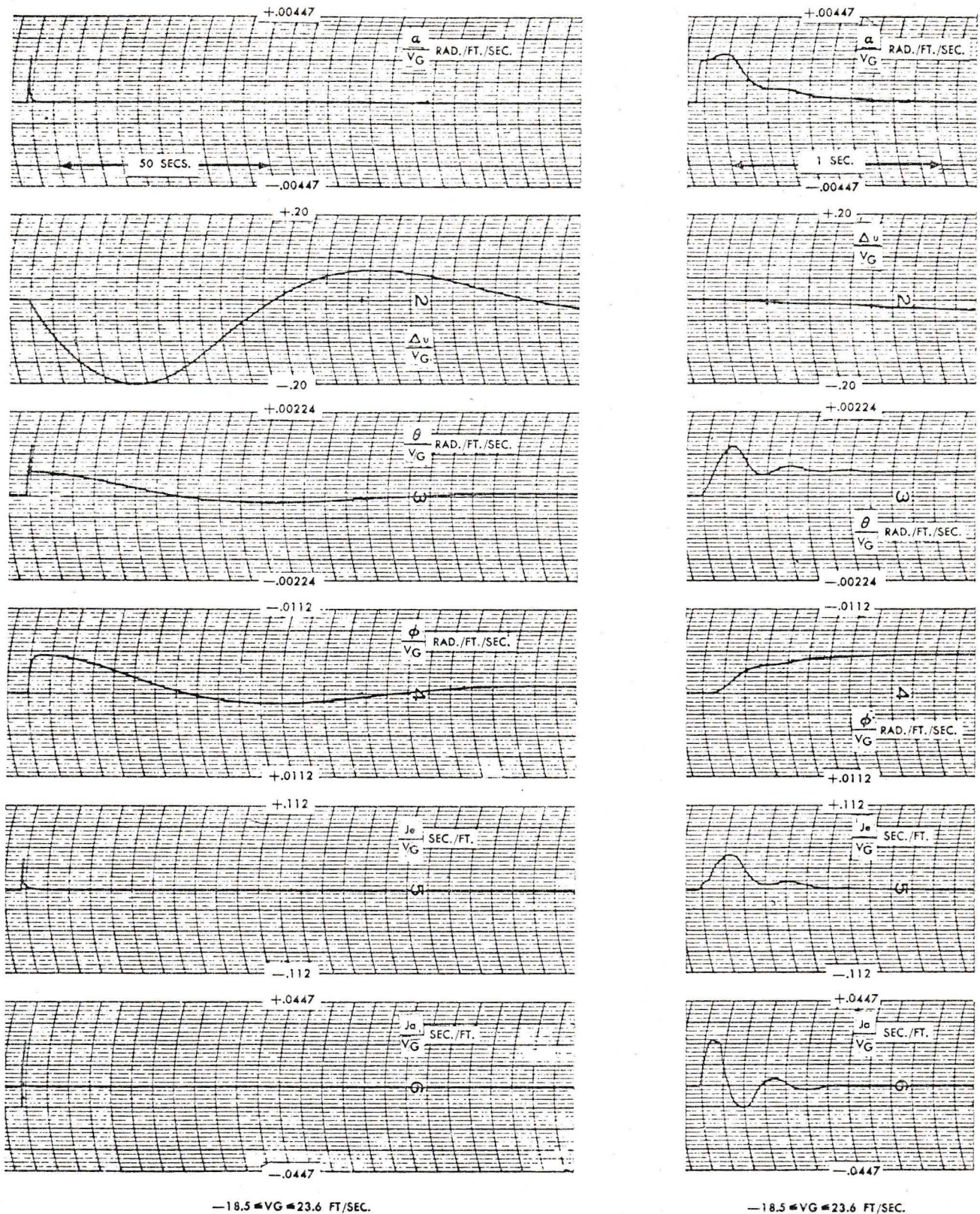
SECRET


 $-31.5 \leq V_G \leq 8.4$ FT/SEC.

 $-31.5 \leq V_G \leq 8.4$ FT/SEC.

M = 0.15

3467-606A-1

FIG. 23 RESPONSE TO A SHARP-EDGED GUST


 $-18.5 \leq V_G \leq 23.6 \text{ FT/SEC.}$
 $-18.5 \leq V_G \leq 23.6 \text{ FT/SEC.}$
 $M = 0.40$

3468-606A-1

FIG. 24 RESPONSE TO A SHARP-EDGED GUST